Journal of Geochemical Exploration 267 (2024) 107578

Contents lists available at ScienceDirect

Journal of Geochemical Exploration

journal homepage: www.elsevier.com/locate/gexplo

Characterization of regolith-hosted rare earth element deposits using reflectance spectroscopy: Framework towards an efficient and reliable field exploration tool

Martin Yan Hei Li [a,b,*], Jiacheng Liu [c], Wei Tan [d], Jia-Xi Zhou [e], Mei-Fu Zhou [a,**]

[a] State Key Laboratory of Ore Deposit Geochemistry, Institute of Geochemistry, Chinese Academy of Sciences, Guiyang 550081, China
[b] School of Applied Sciences, University of Brighton, Brighton BN24GJ, United Kingdom
[c] Department of Earth Sciences and Laboratory for Space Research, The University of Hong Kong, Pokfulam Road, Hong Kong
[d] Key Laboratory of Mineralogy and metallogeny/Guangdong Provincial Key Laboratory of Mineral Physics and Materials, Guangzhou Institute of Geochemistry, Chinese Academy of Sciences, Guangzhou 510640, China
[e] Key Laboratory of Critical Minerals Metallogeny in Universities of Yunnan Province, School of Earth Sciences, Yunnan University, Kunming 650500, China

ARTICLE INFO

Keywords:
Rare earth elements
Regolith-hosted deposits
Reflectance spectroscopy
VNIR-SWIR spectroscopy
Clay minerals
Weathering

ABSTRACT

With a growing demand for the rare earth elements (REE), exploration of regolith-hosted REE resources worldwide has been thriving in recent years and development of a rapid and reliable field-based tool will greatly facilitate the survey and exploration. In this study, we use visible and short-wave infrared (VNIR-SWIR) reflectance spectroscopy to comprehensively evaluate the applicability of the technique to explore regolith-hosted REE resources, exemplified by three representative regolith-hosted REE deposits in China. Neodymium among the REE shows reliably detectable spectral features in the VNIR-SWIR spectroscopy down to concentrations of 10–50 ppm in field samples with heterogeneous mineral grain sizes. The Nd spectral intensity of electronic transition at the band of ~800 nm is correlated with bulk Nd concentrations and can be used as semi-quantitative indicators for the Nd concentrations, thereby the total REE in regolith. Moreover, VNIR-SWIR spectroscopy is demonstrated to be capable of delineating favorable ore-bearing mineralogy by characterizing the abundance and type of clay minerals and Fe (oxyhydr)oxides, and the crystallinity of kaolinite-group minerals. However, the Nd spectral features of samples with high bulk Fe_2O_3 contents (>3 wt%) are significantly masked due to overlapping by the strong absorption features of ferric (oxyhydr)oxides. VNIR-SWIR spectroscopy is deemed to be applicable to the exploration of regolith-hosted REE resources developed from Fe-poor felsic rocks.

1. Introduction

Rare earth elements (REE) are critical resources for the transition to a zero carbon society due to their wide application in many related technologies, such as wind turbines and electric vehicles. A seven-fold increase in demand is forecasted between now and 2040, especially for the more scarce heavy REE (HREE) (IEA, 2021). Regolith-hosted REE deposits are currently the dominant global source of the HREE (Riesgo García et al., 2017). These deposits typically form in tropical and subtropical environment through weathering of granites and felsic volcanic rocks, alkaline rocks, and/or metapelites (e.g., Estrade et al., 2019; Fu et al., 2019; Huang et al., 2021; Li et al., 2019, 2020; Zhou et al., 2020). In regolith-hosted REE deposits, most REE occur in easily exchangeable form adsorbed on clay minerals, including halloysite, kaolinite, illite, and vermiculite (Borst et al., 2020; Li and Zhou, 2020, 2023), for which the adsorption is greatly affected by the crystallinity of the clay minerals (Li and Zhou, 2020; Luo et al., 2024). Part of the REE can also be sorbed on different Fe (oxyhydr)oxides, especially Ce (Huang et al., 2021; Li et al., 2020). Successful exploration of this kind of deposits would be essential to secure the global HREE supply, however, routine exploration strategies require extensive laboratory-based analyses to determine REE concentrations for further survey and drilling. Development of an efficient, economical, and reliable field-based technique would be greatly beneficial to the exploration of the regolith-

* Correspondence to: M.Y.H. Li, School of Applied Sciences, University of Brighton, Brighton BN24GJ, United Kingdom.
** Corresponding author.
E-mail addresses: martinyhli@gmail.com (M.Y.H. Li), zhoumeifu@hotmail.com (M.-F. Zhou).

https://doi.org/10.1016/j.gexplo.2024.107578
Received 12 January 2024; Received in revised form 12 July 2024; Accepted 31 August 2024
Available online 3 September 2024

hosted REE resources, and the recent advance in techniques with visible and short-wave infrared (VNIR-SWIR) reflectance spectroscopy to study REE minerals and deposits highlights the great potential for application to the exploration of regolith-hosted REE resources (e.g., Möller and Williams-Jones, 2018; Neave et al., 2016; Tan et al., 2022; Turner et al., 2014, 2016). The VNIR-SWIR spectroscopy has been recently utilized to study REE minerals (Dijkstra et al., 2024; Turner et al., 2014, 2016, 2018), hard rock-hosted REE deposits (Boesche et al., 2015; Möller and Williams-Jones, 2018; Neave et al., 2016), regolith-hosted REE deposits (Tan et al., 2021; Tan et al., 2022), and REE concentrations of soils (Wang et al., 2017).

Rare earth elements have characteristic absorption bands in the range of visible and near-infrared wavelength (350–1000 nm) (Adams, 1965), due to the *4f-4f* intra-configurational electron transitions (Liu, 2005). Thus, the absorption features of REE are elemental in nature and the intensity of absorption is proportional to concentrations of the specific REE (Clark, 1995), enabling determination of these elements both qualitatively by means of reflectance spectroscopy. Absorption by Fe^{3+} is also achieved through electronic transition in the range of visible and near-infrared wavelength (Cudahy and Ramanaidou, 1997), making it possible to estimate Fe (oxyhydr)oxide abundances based on the absorption intensity. On the other hand, diagnostic features of clay minerals can be identified in the range of short-wave infrared wavelength (1000–2500 nm), based on the vibrational modes of different functional groups (Clark et al., 1990; Hunt, 1977; Hunt and Ashley, 1979; Liu et al., 2021). As an efficient and economical technique, VNIR-SWIR spectroscopy can be used for the exploration of regolith-hosted REE resources, especially when the spectrometer could be mounted on hyperspectral remote sensing platforms, such as unmanned aerial vehicles (UAV) (Booysen et al., 2020), for large-scale field reconnaissance. However, application of VNIR-SWIR spectroscopy to regolith-hosted REE resource exploration is still in the developing stage. To date, there are only two studies to characterize a single regolith-hosted light (L)REE deposits (Renju deposit in South China) with quartz diorite, biotite granite and/or rhyolite tuff as the protolith with VNIR-SWIR spectroscopy (Tan et al., 2021; Tan et al., 2022). Unfortunately, none of them have covered the practical criteria of the technique, including the applicability of the technique to heterogeneous field samples, and resolution and reliability of the spectral results, for potential on-site usage. Moreover, it is uncertain if this technique is applicable to the exploration of regolith-hosted HREE deposits that often develop over muscovite-bearing alkaline granite (Li et al., 2017). To further develop the technique to a rapid and reliable tool for regolith-hosted REE resource exploration, a thorough evaluation on the criteria for applying VNIR-SWIR spectroscopy on field characterization of regolith-hosted REE deposits of varying mineralogical and geochemical properties is necessary.

In this study, three regolith-hosted REE deposits in South China were chosen to test the applicability of VNIR-SWIR spectroscopy for exploration of regolith-hosted REE resources. We comprehensively characterize the REE composition and clay assemblages of these deposits and further to evaluate the suitability of VNIR-SWIR spectroscopy for exploring regolith-hosted REE deposits. We also contrast the powdered samples and the unpowdered counterparts to study the reliability of the technique for the measurement in the field. Further, we summarize the criteria for VNIR-SWIR spectral features to be applicable for semi-quantification of REE concentrations in regolith.

2. Site description

2.1. Zudong deposit

The Zudong deposit in Jiangxi Province, South China, also known as the '701 mine', was discovered in 1969 and was the first regolith-hosted REE deposit identified in China (Xie et al., 2016). This deposit has a current resource of ~18,000 t REO at 0.1 wt% REO (Li et al., 2019). The Zudong deposit was developed via weathering of a late Jurassic two-feldspar, muscovite-bearing alkaline granite (Li and Zhou, 2024) (Fig. 1a). The REE mineralization mainly occurs in the lower pedolith and upper saprolite, with concentrations of REE gradually decreasing from a maximum of ~2000 ppm at the pedolith-saprolite interface towards ~300–350 ppm at both shallower and greater depths, except Ce which has accumulated in the upper pedolith (Li et al., 2019). About 60–70 % of the REE are ion exchangeable and probably adsorbed on clay minerals, dominantly kaolinite and halloysite (Li et al., 2019). The rest of the REE are hosted in residual REE minerals, including xenotime-(Y), zircon and REE niobates, and in supergene minerals, mainly chernovite-(Y). Proportions of REE hosted in secondary Fe—Mn (oxyhydr)oxides and organic matter are negligible (Li et al., 2019).

Overall, the proportion of both kaolinite and halloysite increases from the saprolite and pedolith to the uppermost humic layer, and constitutes 10–30 % of the regolith (Li et al., 2019). Specifically, kaolinite represents ~50–60 % and ~ 70 % of the clay mineral assemblage in saprolite and pedolith, respectively, whereas that of halloysite is relatively higher in the saprolite (~35 %) than in the pedolith (~20 %) and in the humic layer (~5 %). Illite and vermiculite occur in minor proportions (Li and Zhou, 2020). Goethite (up to ~1 %) is a minor component in the pedolith (Li et al., 2019).

2.2. Bankeng deposit

The Bankeng deposit in Jiangxi Province, South China, is a regolith-hosted LREE prospect and has a grade of ~0.15 wt% REO. The deposit formed from a Triassic two-feldspar, biotite-bearing granite (Fig. 1a). The maximum REE concentration of ~1500 ppm occurs in the lower pedolith and upper saprolite, while Ce decouples from the other REE and show exceptional enrichment at the saprolite-saprock interface (Li et al., 2020). Up to 60 to 80 % of the REE occur in ion exchangeable form (Li et al., 2020), except Ce that shows a much stronger affinity to the Fe—Mn (oxyhydr)oxides. Nearly all and ~ 70 % of bulk Ce are bound to Fe—Mn (oxyhydr)oxides at the saprolite-saprock interface and the pedolith-saprolite interface, respectively. Other REE are presumed to be mainly adsorbed on kaolinite and halloysite, and sub-ordinately on illite in the saprolite and vermiculite in the pedolith, particularly for the HREE (Li and Zhou, 2023). There are only minor amounts of REE bound to the organic matter, except Ce that up to 10 % of the bulk concentration could be sorbed on organic matter. The remaining 10–20 % of the bulk REE are hosted in residual monazite, zircon, and secondary rhabdophane and cerianite (Li et al., 2020).

Kaolinite and halloysite are the main clay minerals in the Bankeng regolith, constituting ~5–25 % of the regolith (Li et al., 2020). A detailed characterization reveals that kaolinite and halloysite comprise ~70 % of the clay mineral assemblage, illite constitutes up to 20 %, especially in the saprolite and vermiculite is up to 20 %, especially in the pedolith (Li et al., 2021). Bulk regolith analysis did not detect any Fe (oxyhydr)oxide phases of >1 % (Li et al., 2020).

2.3. Puxiong deposit

The Puxiong deposit in Yunnan Province, Southwest China, is a regolith-hosted deposit formed through weathering of a nepheline syenite (Fig. 1b). The deposit hosts a resource of 47,000 t REO at a grade of ~0.15 wt% (Wang et al., 2024). Compared to the other deposits formed via weathering of granite, ore bodies of the Puxiong deposit, with REE concentration of up to 10,000 ppm, are confined to shallower depth in the pedolith and are generally thinner. Kaolinite and halloysite are the main clay minerals in the hilltop regolith and the proportion increases from ~40 % in saprolite to ~65 % in pedolith. Illite also exists and the proportion varies between 2 and 60 %. A small amount of gibbsite and vermiculite occur in the uppermost regolith. The abundances of Fe (oxyhydr)oxides are generally low (<5 %) but could be locally up to 25 %. Halloysite and illite are regarded as the main REE sorbents in the regolith, and a minor amount of REE is hosted in rhabdophane and Fe-

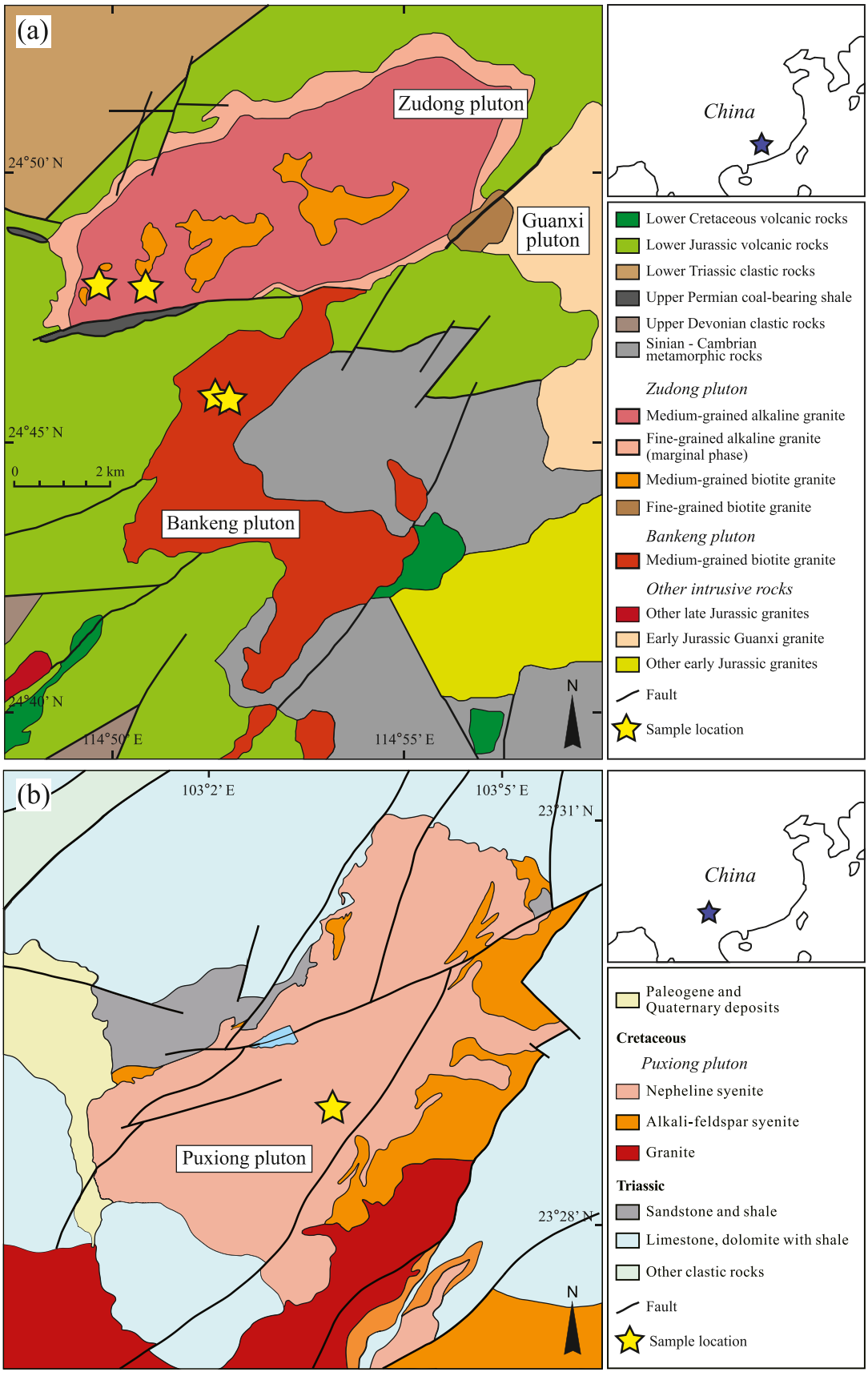

Fig. 1. Simplified geological maps of (a) Zudong and Bankeng deposits (after Li et al., 2019, 2020) and (b) Puxiong deposit (after Wang et al., 2024).

Mn-REE (oxyhydr)oxide phases (Wang et al., 2024).

3. Methodology

3.1. Samples

In this study, 54 samples from the Zudong deposit, 77 from the Bankeng deposit, and 67 from the Puxiong deposit are analyzed to obtain the VNIR-SWIR spectral features. The bulk mineralogical and geochemical compositions of some samples from Zudong and Bankeng are published in Li et al. (2019) and Li et al. (2020), respectively. An additional 14 samples from Zudong, 24 samples from Bankeng are included in this study. All samples from Puxiong are analyzed in this study. These samples are taken from 2 profiles at the Zudong deposit (Profiles LN-1 and LN-2); 5 profiles at the Bankeng deposit (Profiles BK-R at the ridgetop, BK-U at the upslope, and BK-F1, BK-F2 and BK-F3 at the footslope of an ore-bearing catchment); and a 90-m-long drill core at the Puxiong deposit.

3.2. Major mineral abundance analysis

The major minerals were identified and their abundances semi-quantified by Micro Structure Analytical Laboratory of Peking University. Samples were ground to a fine powder and pestled and analyzed with a Bruker D8 Advance powder X-ray diffractometer. Each sample was X-rayed with non-monochromated Cu Kα radiation (40 kV, 40 mA) from 2° to 70° 2θ at a scanning speed of 2° per minute. The diffractograms were analyzed and the proportions of the different minerals were semi-quantitatively determined through a Rietveld refinement with the reference intensity ratio methods (cf. Tamer, 2013) using the JADE 6.5 software.

3.3. Bulk major and trace element analysis

The bulk major and trace element contents were analyzed by ALS Chemex (Guangzhou) Co. Ltd. The major element contents were measured using wavelength-dispersive X-ray fluorescence spectrometry (WD-XRFS) on fused glass beads. Accurately weighted samples were dried at 105 °C, and then fused with lithium tetraborate in a 1:10 ratio to prepare glass beads for analysis. Loss of ignition (LOI) was determined after combustion of the weighted samples at 1000 °C. The analysis was undertaken with an PANalytical PW2424 XRFS instrument, which has an analytical accuracy and precision of <5 % for major element oxides.

Trace element concentration analysis was conducted on samples digested with two different procedures. Two equivalent batches of samples were accurately weighted, one being digested with a mixture of $HClO_4$-HNO_3-HF, dried, and re-dissolved in dilute HNO_3 for analysis, and the other batch being fused with lithium tetraborate at 1025 °C, and dissolved in a mixture of HNO_3-HCl-HF for analysis. Measurement was done with an Agilent 7900 inductively coupled plasma mass spectrometer (ICP-MS). The reported results are the average of the measurements on samples digested in two different procedures. Errors for both the accuracy and precision were < 10 % for all elements analyzed.

3.4. Visible and short-wave infrared (VNIR-SWIR) reflectance spectroscopy

Both powdered and unpowdered regolith samples were measured with an Analytical Spectral Devices FieldSpec-4 spectrometer at the Guangzhou Institute of Geochemistry, Chinese Academy of Sciences. The measurement was performed in a dark room under a standard atmosphere using a circular detector with the spot size of approximately 20 mm. The reflectance measured on a white plate is adopted as the background. Each measured spectrum was acquired by averaging 200 scans to improve the signal-to-noise ratio. The spectral resolution is 3 nm (fullwidth-half-maximum) at 700 nm, 10 nm at 1400 nm, and 10 nm at 2100 nm. The sampling interval is 1.4 nm for the spectral region 350–1000 nm, and 2 nm for the spectral region 1000–2500 nm.

The ViewSpecPro software was used to preprocess the raw spectra, including splice correction and averaging. Phase identification was achieved by comparing the reference spectra from the Analytical Spectral Devices spectra library. Although there may be a 1- to 3-nm differences in the values of VNIR-SWIR absorption bands from analyses of the same mineral with different instruments, the produced trends and patterns are generally consistent with each other (Chang and Yang, 2012). Afterwards, the raw spectra were processed using The Spectral Geologist (TSG™; https://research.csiro.au/thespectralgeologist/tsg/) software to remove the background noise and to isolate specific absorption features for identification and analysis using the continuum removal approach. In TSG, the Fourier self-deconvolution approach is used to locate the position center (wvl; i.e., the wavelength at which the fitted spectra reach the minimum) and to acquire the band depth (BD; i.e., the distance from baseline to peak) of specific absorption band. The second derivative curves of the raw spectra were derived to detect any slight changes in the original reflectance spectrum (Mathian et al., 2018), and the maxima (M) obtained from the second derivative curves represent the inflection points on VNIR-SWIR spectra and are proportional to the intensities of given bands on the raw spectra.

3.5. Extraction of mineralogical and geochemical information

The spectral data are further processed to determine spectral indices characterizing the mineralogical and geochemical properties of the regolith, including the clay minerals, Fe (oxyhydr)oxides, and REE concentration. The spectral indices extracted in this study are elaborated in this section and summarized in Table 1.

3.5.1. Clay minerals

Clay minerals show characteristic spectral absorptions at ~1400 nm for the 1st overtone of OH stretching vibration (υOH) and at ~2200 nm for a combination of υOH and the Al-OH bending vibration (δAlAl-OH). An additional adsorption feature at ~1900 nm would be shown if interlayer molecular water exists (e.g., smectite), contributed by the combination of υOH and the HOH bending vibration (Bishop et al., 2008; Clark et al., 1990; Hunt, 1970). Therefore, the BD of these absorption bands are positively correlated with the abundance of clay minerals (for the ~1400 and ~ 2200 nm wavelengths) and H_2O-bearing clay minerals (for the ~1900 nm wavelength). To distinguish between kaolinite and illite, the two major clay minerals in these deposits (Li et al., 2019; Wang et al., 2024), BD2350 is applied as white mica shows spectral adsorption at ~2350–2370 nm for υ + δMgMgMg-OH but not for kaolinite (Bishop et al., 2008). Furthermore, in Haest et al. (2012), spectral index 2160D2190 based on four-band ratio over 2160 to 2180 nm wavelength region to distinguish between kaolinite-group minerals and non-kaolinite group minerals, index 2350De based on four-band ratio for the absorption at ~2350 nm to distinguish between muscovite/illite and smectite, and an index based on a six-band ratio over the 2140 to 2190 nm wavelength region (denoted as 2140D2190 here) for different types of kaolinite-group minerals and the degree of kaolinite crystallinity have been developed.

3.5.2. Fe (oxyhydr)oxides

Fe (oxyhydr)oxides can also produce diagnostic spectral absorption in VNIR-SWIR spectra due to the electronic processes by Fe^{3+} octahedrally bonded to oxygen (hematite) or oxygen and hydroxyl (goethite and other Fe^{3+} hydroxides) (Sherman and Waite, 1985). In general, the absorptions at 520–550 and 860–890 nm are characteristics of hematite, while those at 400–480 and 915–960 nm are of goethite (Cudahy and Ramanaidou, 1997; Hunt and Ashley, 1979; Liu et al., 2021; Rowan et al., 1986). As the 2nd overtone of OH stretching vibration of the clay minerals at ~960 nm could impose significant overlapping of the Fe^{3+} absorption in 860–960 nm wavelength region, the BD of the absorption

Table 1
Summary of spectral indices applied in this study.

Spectral index	Index name	Calculation script	Geological indications	Reference
BD500	Fe^{3+} intensity I	BD500 = 1-R530/(0.483*R614 + 0.517*R440)	High value indicates higher Fe^{3+} content	Viviano et al. (2014)
BD900	Fe^{3+} intensity II	BD900 = 1-R920/(0.362*R807 + 0.638*R984)	High value indicates higher Fe^{3+} content	Viviano et al. (2014)
BD1400	Hydroxyl intensity	BD1400 = 1 - R1415/(0.394*R1330 + 0.606*R1467)	High value indicates more hydroxyl in clay minerals	Viviano et al. (2014)
BD1900	Interlayer water intensity	BD1900 = 1 - R1915/(0.705*R1850 + 0.295*R2067)	High value indicates higher abundance of interlayer water-containing clay minerals (e.g., smectite)	Viviano et al. (2014)
BD2200	Al-OH intensity	BD2200 = 1 - R2207/(0.506*R2165 + 0.494*R2250)	High value indicates more Al-OH group in TO or TOT type clay minerals	Viviano et al. (2014)
BD2350	MgMgMg-OH intensity	BD2350 = 1 - R2356/(0.36*R2340 + 0.64*R2365)	High value indicates higher abundance of white micas (e.g., muscovite and illite)	Modified after Viviano et al. (2014)
BD1400/BD1900	Weathering intensity I	Ratio of BD1400 to BD1900	Intensity ratio between OH and interlayer water; high value indicates higher weathering intensity	Liu et al. (2021)
BD2200/BD1900	Weathering intensity II	Ratio of BD2200 to BD1900	Intensity ratio between Al-OH and interlayer water; high value indicates higher weathering intensity	Liu et al. (2021)
2160D2190	Separation of kaolinite-group minerals from non-kaolin Al silicates	2160D2190 = (R2136 + R2188)/(R2153 + R2171)	Kaolinite-group mineral is more abundant than the other non-kaolin Al silicates when 2160D2190 > 1.005	Haest et al. (2012)
2140D2190	Type and crystallinity of kaolinite-group minerals	2140D2190 = [(R2138 + R2173)/R2156]/[(2155 + 2190)/2173]	Higher value indicates lower crystallinity	Haest et al. (2012)
2350De	Separation of illite from Al-smectite	2350De = (R2326 + R2376)/(R2343 + R2359)	Illite is more abundant than Al-smectite when 2160D2190 < 1.005 and 2350De >1.02	Haest et al. (2012)
M797-M785	Nd^{3+} intensity I	The maximum at 797 nm minus the minimum at 785 nm in the second derivative curve	High value indicates higher Nd^{3+} content	This study
M742-M730	Nd^{3+} intensity II	The maximum at 742 nm minus the minimum at 730 nm in the second derivative curve	High value indicates higher Nd^{3+} content	This study
M1390	Kaolinite-group mineral intensity	The maximum between 1380 and 1400 nm in the second derivative curve	High value indicates higher abundance of kaolinite-group minerals	Tan et al. (2022)
500 wvl	Fe^{3+} wavelength	Peak position of reflectance minimum of continuum removed wavelength of fourth-order polynomial fitted between 400 and 600 nm	Relative abundance of hematite is higher when peak position is at >500 nm, and goethite and other Fe (III)-rich minerals is higher when peak position is at <500 nm	Cuadros et al. (2020)

at ~500 nm is often adopted to estimate the abundance of Fe (oxyhydr) oxides (e.g., Tan et al., 2022). Further, the peak position of the reflectance minimum at ~500 nm is also utilized to determine the relative abundance of hematite and goethite (Cuadros et al., 2020).

3.5.3. REE concentration

Owing to the *4f* electronic configuration, REE except La^{3+}, Lu^{3+}, Y^{3+}, and Ce^{4+}, could show absorptions in VNIR-SWIR spectra. The position of the absorption bands would vary slightly depending on the coordination environment and asymmetry of REE in different minerals and phases (Turner et al., 2014). VNIR-SWIR absorptions bands of REE could be notably detected on Pr^{3+}, Nd^{3+}, Sm^{3+}, Eu^{3+}, and Tb^{3+} (Möller and Williams-Jones, 2018; Turner et al., 2018; Wang et al., 2017), while those derived from Dy^{3+}, Ho^{3+}, Er^{3+}, Tm^{3+}, and Yb^{3+} often overlap with the absorption bands of Fe in Fe-bearing (oxyhydr)oxides and clay minerals (Cudahy and Ramanaidou, 1997; Turner et al., 2018) and thus, are often hardly detected (Tan et al., 2021). In regolith-hosted REE deposits, the concentrations of Pr, Eu, and Tb are often too low to be detected by VNIR-SWIR spectroscopy (e.g., Tan et al., 2022). Alternatively, Nd often shows obvious absorption bands at ~580, 740, 800, and 865 nm (Möller and Williams-Jones, 2018; Neave et al., 2016; Tan et al., 2021; Tan et al., 2022; Turner et al., 2014, 2016, 2018). Tan et al. (2022) demonstrated that the processing of spectra with the second derivate method could significantly enhance the signals, thus the same approach is adopted here to extract the spectral features of Nd. In the second derivative curves, the maxima would be correlated to the intensity of absorption at the corresponding wavelength, while the minima immediately adjacent to it would represent the intensity of the background (cf. Mathian et al., 2018; Tan et al., 2021; Tan et al., 2022). As the minima are often not zero and the absolute values vary among samples, to normalize the data among samples for comparison, the difference between the maxima and the associated minima is adopted here to present the spectral intensity.

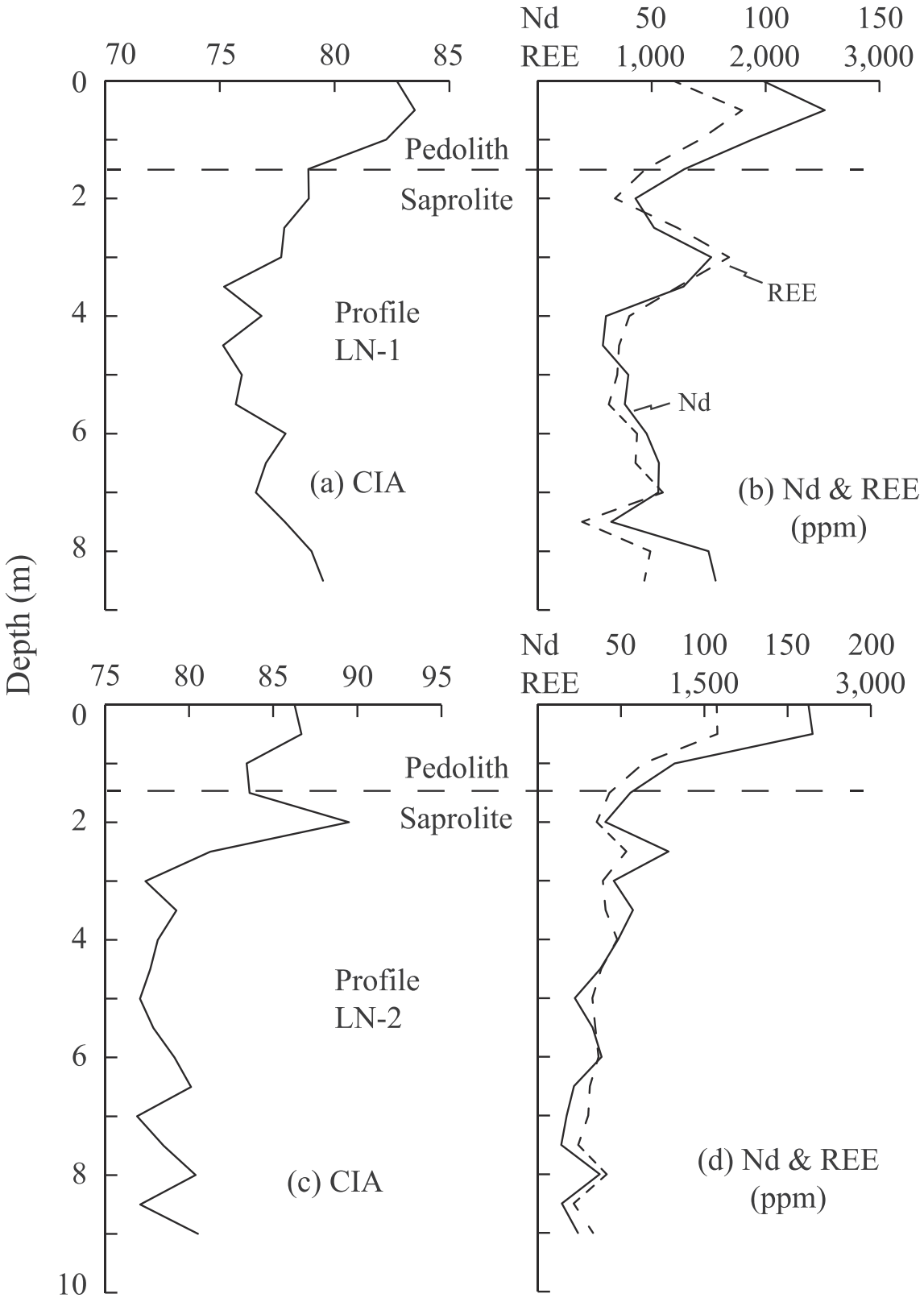

Fig. 2. Variation of CIA, Nd (in solid line) and REE (in dash line) concentrations in Profiles LN-1 and LN-2 from the Zudong deposit.

4. Results

4.1. Mineralogical and chemical composition

4.1.1. Zudong deposit

The samples are collected in the lower pedolith and saprolite of the previously studied profile by Li et al. (2019). Results are presented in Table S1 and Fig. 2. The Chemical Index of Alteration (CIA = $[Al_2O_3/(Al_2O_3 + CaO\ [silicate] + Na_2O + K_2O)] \times 100$) of these samples ranges from 75 to 82 (Fig. 2a, c). The REE concentrations vary between ~450 and ~ 1800 ppm, Nd concentration between 20 and 120 ppm (Fig. 2b, d), and $(La/Yb)_N$ ratio between 0.2 and 0.6. Trends of variation of Nd concentration in the profiles largely mimic those of the whole REE concentration. All the samples are HREE-enriched, in consistency with the previous studies on the same deposit (Li et al., 2019).

4.1.2. Bankeng deposit

Two weathering profiles at the footslope of the ore-bearing catchment studied in Li et al. (2020) have been sampled to supplement the dataset in this study. Results are presented in Table S2 and Fig. 3. In general, both profiles show regolith from upper pedolith to middle or lower saprolite (transition zone not exposed). The CIA values of both profiles show gradual decreases from ~75–80 at top to ~65 at bottom (Fig. 3a, c). In both profiles, the REE concentration gradually increases from the uppermost soil (Profile BK-F2: REE of 330 ppm, Nd of 45 ppm; Profile BK-F3: REE of 130 ppm, Nd of 10 ppm) the maximum at the pedolith-saprolite interface (Profile BK-F2: REE of 520 ppm, Nd of 100 ppm; Profile BK-F3: REE of 650 ppm, Nd of 120 ppm). REE concentrations are lower in saprolite (Profile BK-F2: REE of 350–400 ppm, Nd of 50–60 ppm; Profile BK-F3: REE of ~300 ppm, Nd of 50 ppm), except the sample collected at the bottom of the profile (Profile BK-F2: at depth of 6.5 m, of 470 ppm, Nd of 80 ppm; Profile BK-F3: at depth of 4.1 m; REE of 480 ppm and Nd of 70 ppm) (Fig. 3b, d). The $(La/Yb)_N$ ratio gradually increases from the top (~10) to the bottom (~28) in Profile BK-F2, but increases from the uppermost soil (~4) to the lower pedolith (20–25) and then decreases in the saprolite (15–18) in Profile BK-F3. All the samples are LREE-enriched, in consistency with the previous studies on the same deposit.

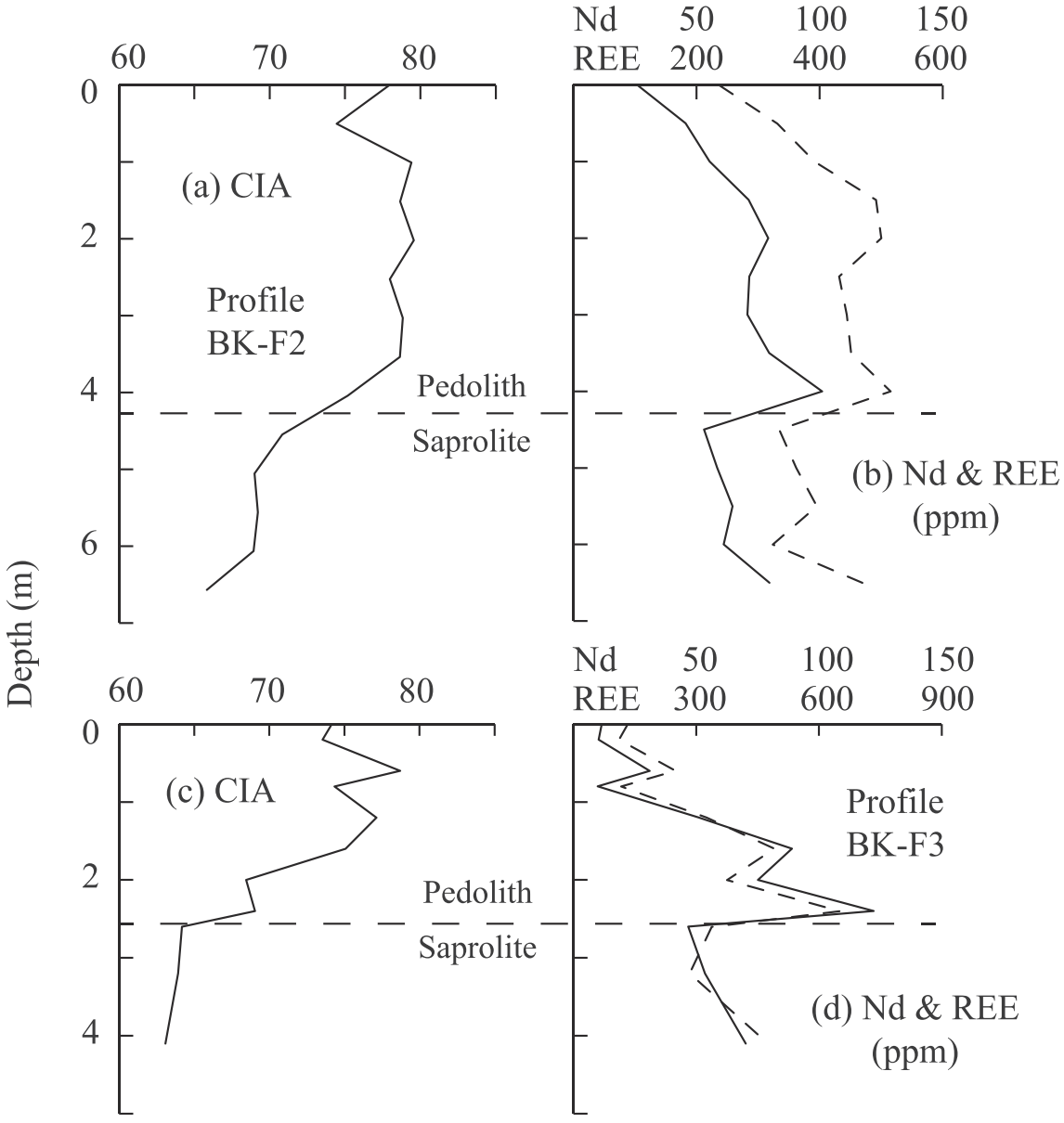

Fig. 3. Variation of CIA, Nd (in solid line) and REE (in dash line) concentrations in Profiles BK-F2 and BK-F3 from the Bankeng deposit.

4.1.3. Puxiong deposit

The profiles studied here show clear zonation, from top to bottom, of the humic layer (thickness of 0.7 m), the pedolith layer (thickness of 25 m), and the saprolite (thickness of >65 m). Results are presented in Table S3 and Fig. 4. Kaolinite-group minerals and illite, and, illite and microcline are the major minerals in the pedolith and saprolite, respectively (Fig. 4a). In the pedolith, the abundance of kaolinite-group minerals varies between 20 % to near 100 %, and in general, increases from the topsoils to the middle pedolith, at the depth of 15–16 m, and then decreases towards the pedolith-saprolite interface. The variation of illite abundance slightly fluctuates from 5 to 10 % in the upper pedolith, increases to 30–60 % in the middle pedolith and finally decreases to <15 % in the lower pedolith, except in the topsoil where up to 30 % of illite could be found. The occurrence of smectite and gibbsite is largely restricted to the topsoil of 5–10 % and 10–20 %, respectively. Notably at the depth of ~3 m, an extraordinarily high gibbsite abundance of ~40 % is detected in the regolith. Goethite occurs in a few percent in the upper pedolith and is not detected in the lower pedolith. In the saprolite, microcline generally proportionate 30–60 %, and kaolinite-group minerals of 10–45 %. Illite abundance varies coherently of 40–45 % throughout the entire saprolite, except at 30–35 m and 48–52 m where the abundance significantly drops to <15 %. Up to 5 % of goethite is common in the saprolite.

Geochemically, the CIA index slightly increases from 92 in the topsoil to 95–100 in the upper and middle pedolith, and then gradually decreases to 86 in the lower pedolith, and further to 75–80 in the upper saprolite. Saprolite of the remaining profile shows an CIA index from 65 to 70 (Fig. 4b). Both, the whole REE and Nd concentrations, show the same pattern in the profile (Fig. 4c). REE concentration of the pedolith varies greatly between 650 and 3000 ppm (40–450 ppm for Nd) and exhibits as a couple of concentration peaks in the upper pedolith. The maximum REE concentration of ~9000 ppm (840 ppm for Nd) is detected at the middle pedolith. The lower pedolith has REE concentration of 1200 ppm (150 ppm for Nd) and that increases to 2400 ppm (350 ppm for Nd) at the pedolith-saprolite interface. In the saprolite, the REE concentration is of 1600–2000 ppm (160–200 ppm for Nd) and another concentration peak of 4000 ppm (420 ppm for Nd) occurs at the depth of ~40 m. The REE concentration of regolith below that depth is generally of <1000 ppm (<100 ppm for Nd), except at the depth of 75–80 m. The $(La/Yb)_N$ ratio of the regolith dramatically varies from 10 to 160, but generally follows the pattern of the REE concentrations and higher $(La/Yb)_N$ ratios are associated with higher REE concentrations.

4.2. Spectral features

Representative spectra from the three deposits are given in Figs. 5 to 7, and the spectral indices determined for all the samples are tabulated in Table S4 and S5, and presented in Figs. S1 to S8.

4.2.1. Clay minerals

In all three deposits, VNIR-SWIR absorptions at 1415, 1915, 2207 and 2356 nm, are exhibited (Figs. 5–7). A doublet band at ~1390 nm is well observed for the Zudong samples and for most of the Bankeng and Puxiong samples. Alternatively, a shoulder extending to 1390 nm from the 1415 nm band is observed for the other Bankeng and Puxiong samples. The 1915 nm band appears as a single absorption feature in all samples while the 2207 nm band is often associated with a well-defined shoulder extending to 2170 nm except for a few Puxiong samples, the shoulder of which is broad and gradually transits to the background. The absorption at 1390 nm can be due to the 1st overtone of the stretching vibration of the inner-surface hydroxyl group of kaolinite, whereas the absorption at 2170 nm can be attributed to the combination of Al-OH fundamental stretching and bending vibrations of kaolinite (Bishop et al., 2008). This indicates that kaolinite-group minerals are major component in the regolith. The further application of the 2160D2190 index also shows that the kaolinite-group minerals would be more abundant than the other Al-clay minerals (Table S4 and S5), except near the bottom of the Bankeng footslope profiles (Profiles BK-F1, BK-F2 and BK-F3) and the Puxiong profile. Interestingly, some powdered samples, at various depth from the Bankeng footslope profile and mainly at the lower part of the Puxiong profile show the 2160D2190 indices smaller than 1.005, suggesting the dominance of non-kaolinite-group Al-OH clay minerals that is contradictory to the results from the regolith samples. However, these powdered samples, especially those from the upper part of the Bankeng footslope profile, are of 1.001–1.005 (Table S5) that may not be decisive to confidently distinguish between the two groups. The adsorption band at 2356 nm is generally weak and can be due to the combination of Mg-OH fundamental stretching and bending vibrations of white micas (Bishop et al., 2008). For the non-kaolinite group Al-OH clay minerals as defined by the 2160D2190 index, the non-kaolinite group Al-OH clay minerals all have the 2350De values lower than 1.02, indicating that they are mainly Al-smectite (Haest et al., 2012).

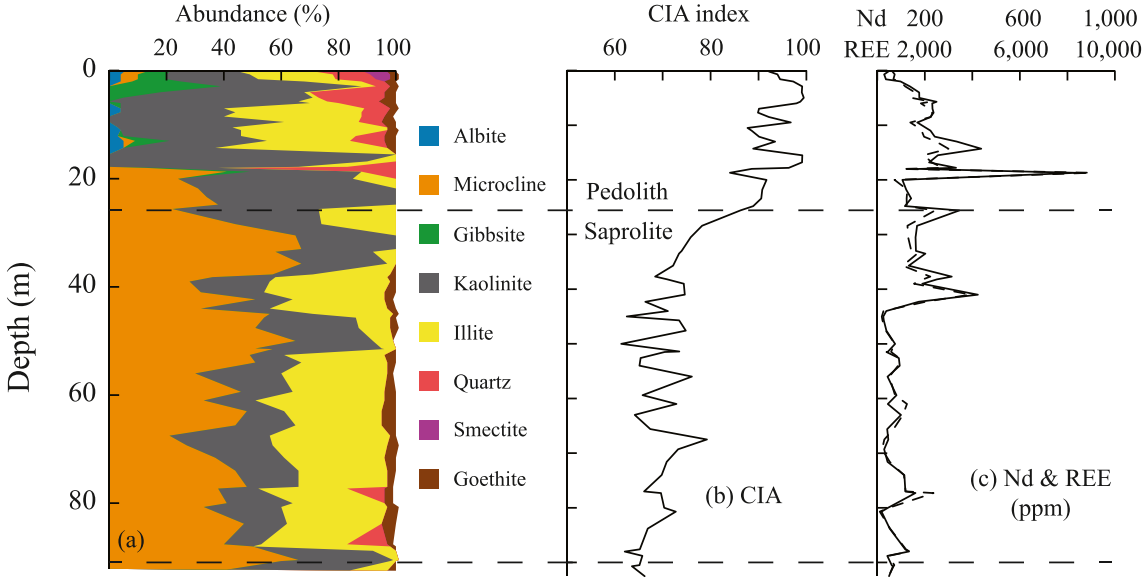

Fig. 4. Variation of mineralogical composition, CIA, Nd (in solid line) and REE (in dash line) concentrations in the profile from the Puxiong deposit.

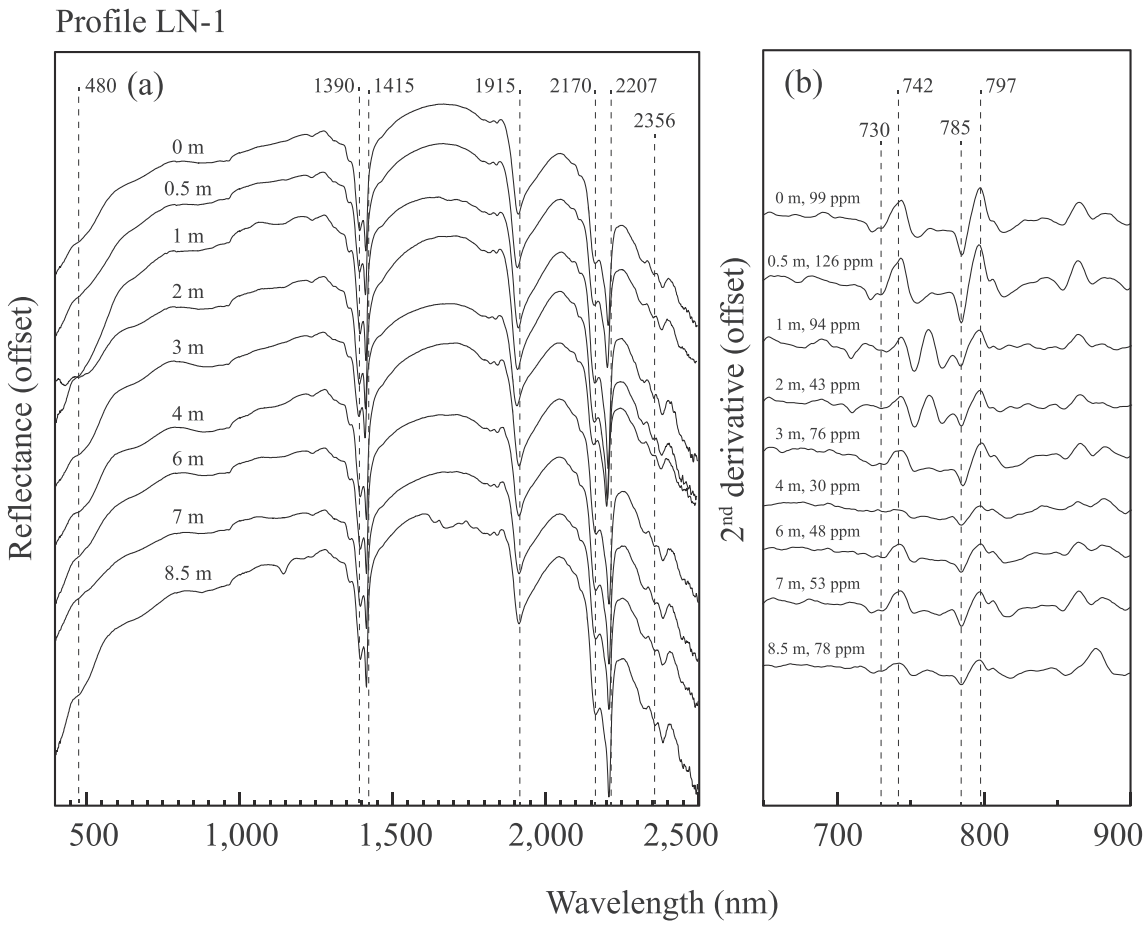

Fig. 5. Representative (a) visible and short-wave infrared reflectance spectra and (b) corresponding second derivative curves from the Zudong deposit. The depth of sample and Nd concentration in (b) are also provided.

4.2.2. *Fe (oxyhydr)oxides*

Generally, BD500 values are much higher and much more varying than the corresponding BD900 values of the same sample. The comparative study suggests that the BD500 values of the powdered samples often show greater variation in the same profile relative to the unpowdered samples. The variation of the BD 500 values exhibits a parabolic shape with an increasing trend with depth first and followed by a decreasing trend towards lower saprolite in profiles LN-1 (Zudong deposit) and BK-F1, F2 and F3 (Bankeng deposit). However, the variation is slight for other studied profiles. At the Puxiong deposit, the BD500 values shows a similar parabolic trend in the pedolith but much more fluctuating pattern in the saprolite. The 500 wvl index indicates that goethite is relatively more abundant than hematite in the entire profile, except a single sample in the saprolite at the depth of ~50 m.

4.2.3. *Nd^{3+}*

Processing of the second derivative curves has detected Nd^{3+} absorption bands at 742 and 797 nm (Figs. 5–7), approximately corresponding to the Nd^{3+} absorption at ~740 and 800 nm in bastnäsite (Turner et al., 2016). The absorption bands of Nd^{3+} at ~580 and 865 nm that are observed in Möller and Williams-Jones (2018); Neave et al. (2016) are not observed in this study. Likewise, the absorption bands corresponding to other REE determined in previous studies (e.g., Tan et al., 2021) are not detected in this study. The second derivative processes spectra of Nd^{3+} show a single peak derived from the absorption at approximately 797 nm and a single peak, occasionally with a shoulder, derived from the absorption at approximately 742 nm. These two peaks are associated with the minima at 785 and 730 nm, respectively, such that the obtained differences between the maxima and minima would be M797-M785 and M742-M730. The M797-M785 values are generally much higher than the corresponding M742-M730 values, and those measured from the unpowdered samples are generally higher than those from the corresponding powdered samples. In Zudong deposit, both values apparently gradually decrease with depth while in the Bankeng deposit, both values mimic a parabolic trend to increase first but then decrease with depth after beyond the pedolith-saprolite interface for the unpowdered samples. In general, the powdered samples could not provide a certain trend for these values. In the Puxiong deposit, the M797-M785 value from the unpowdered samples define a parabolic trend in the pedolith, followed by another similar trend from the lower pedolith to upper saprolite. The value is overall consistent in the rest of the saprolite. The M742-M730 value could not define a clear trend, nor both values from the powdered samples.

5. Discussions

5.1. *Mineralogical and geochemical variations*

Profile-wise, vertical mobilization would cause leaching of elements in upper pedolith and accumulation in lower pedolith and upper saprolite. The pedolith-saprolite interface denotes the weathering front across which the weathering potential of the soil solutions dramatically decreases, and very often, is associated with an increase in soil pH to cause mineral precipitation and/or element adsorption on clay minerals and Fe (oxyhydr)oxides (Nesbitt and Young, 1989). At all three studied sites, the CIA index shows an abrupt decrease across the pedolith-saprolite interface (Figs. 2–4), revealing a significant increase in weathering intensity when saprolite is transforming into pedolith.

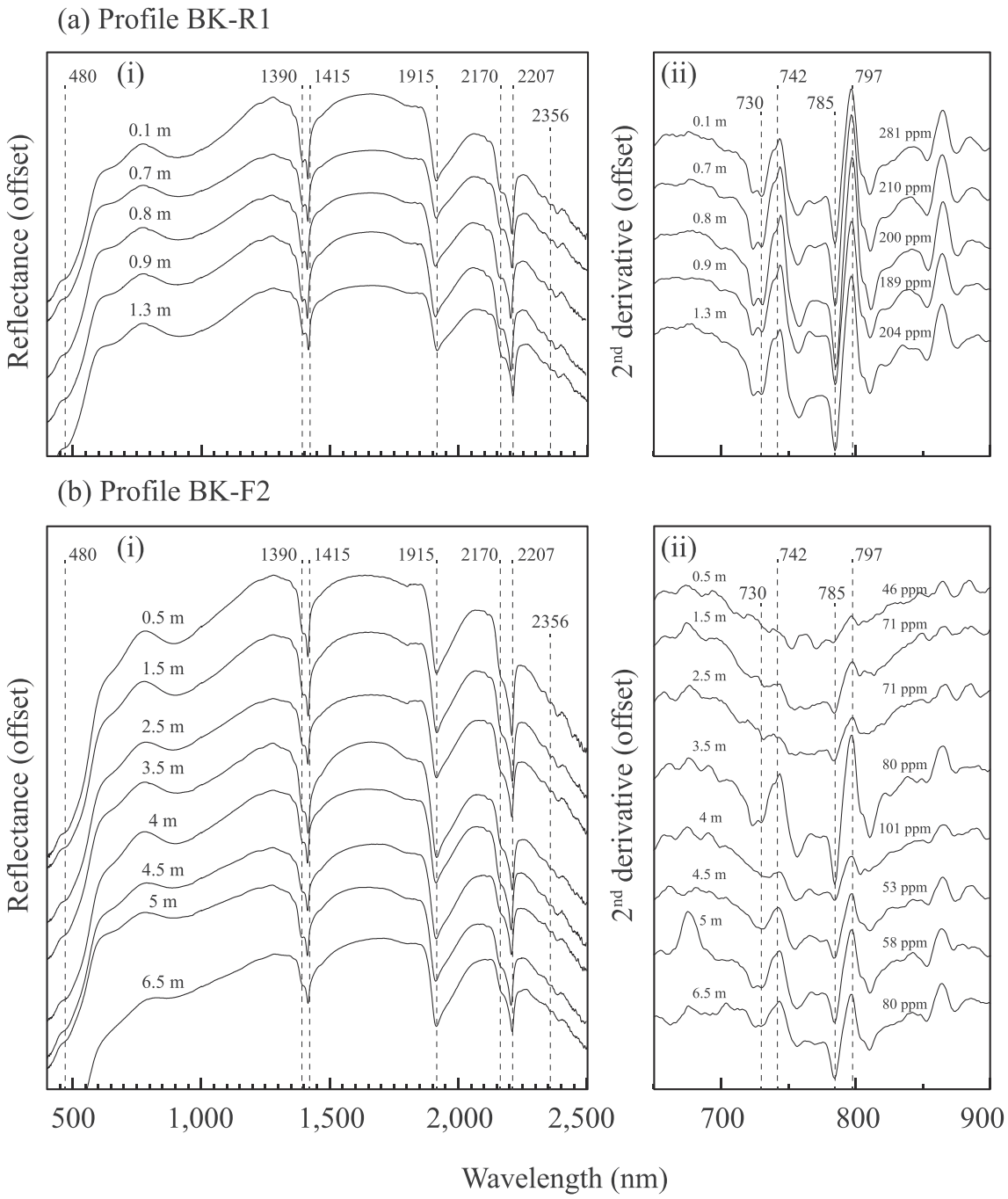

Fig. 6. Representative (a) visible and short-wave infrared reflectance spectra and (b) corresponding second derivative curves from the Bankeng deposit. The depth of sample and Nd concentration in (b) are also provided.

Coherently, the maximum REE enrichment is observed at this interface for the Zudong and Bankeng profiles (Figs. 2 and 3), further suggesting that changes in soil pH and weathering intensity could be the reasons for the REE enrichment. Adsorption of REE on clay minerals, such as kaolinite and halloysite, generally increases with increasing pH (Coppin et al., 2002; Yang et al., 2019) and furthermore, recrystallization of highly defected clay minerals of large surface area and high adsorption capacity with weathering would cause REE desorption in more weathered pedolith (Li and Zhou, 2020, 2023; Luo et al., 2024). The combination of these two factors could cause the REE enrichment preferentially in the lower pedolith and upper saprolite, as observed from the studied profiles.

However, the REE trend is different at the Puxiong deposit, of which the maximum REE enrichment occurs shallower in the pedolith (Fig. 4). As suggested by Wang et al. (2024), due to the lack of coarse-grained quartz and fine-grained nature, regolith generated from weathering of syenite have relatively lower permeability than those derived from granite. The retardation of soil solution infiltration is likely the reason for REE accumulation to take place at shallower pedological depth of the profiles. Progressive weathering would decompose K-feldspar to form illite and further to kaolinite (Meunier, 2005). That explains the high abundance of illite in the saprolite and succeeded by kaolinite in the pedolith. Nonetheless, at certain samples from the pedolith, high contents of illite were still detected. One possibility would be external input from hillslope process. Minor amounts of albite and varying amounts of quartz were also detected in the pedolith (Fig. 4a). Considering that

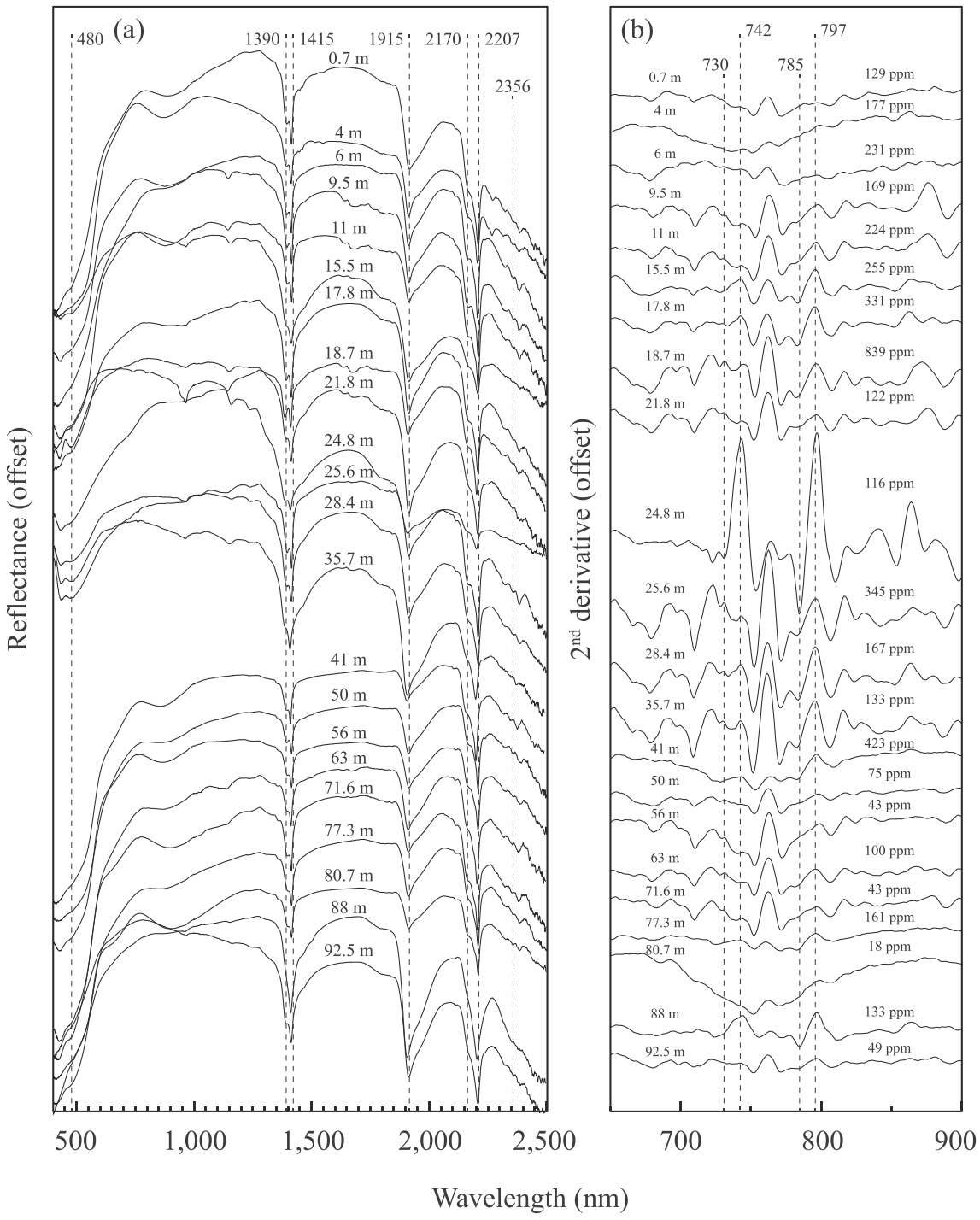

Fig. 7. Representative (a) visible and short-wave infrared reflectance spectra and (b) corresponding second derivative curves from the Puxiong deposit. The depth of sample and Nd concentration in (b) are also provided.

albite is highly weatherable and absent in the saprolite, it is unlikely for any in-situ albite to survive the more intense weathering in the pedolith. Moreover, the amount of quartz should gradually increase with increasing weathering intensity if the quartz is in-situ. Therefore, external input to the pedolith of the Puxiong profile is probable, and that may explain the occurrence of relatively high abundance of illite in some samples from this horizon (Fig. 4a).

5.2. Spectral proxies for potential REE sorbents

5.2.1. Clay minerals

In all three deposits, Al-OH clay minerals, including kaolinite-group minerals and illite, dominate the supergene phyllosilicate assemblage. Comparing the spectral indices BD2200 and BD1400 with the total amount of Al-clay minerals determined from QXRD, very different correlations are obtained in each deposit. Poor correlations ($r^2 < 0.2$) are shown for the Zudong deposit (Fig. 8a), but moderate correlations are shown for the Bankeng deposit ($r^2 = 0.46$ against BD2200 and 0.58 against BD1400) (Fig. 8b). Moderate correlation is also exhibited for the

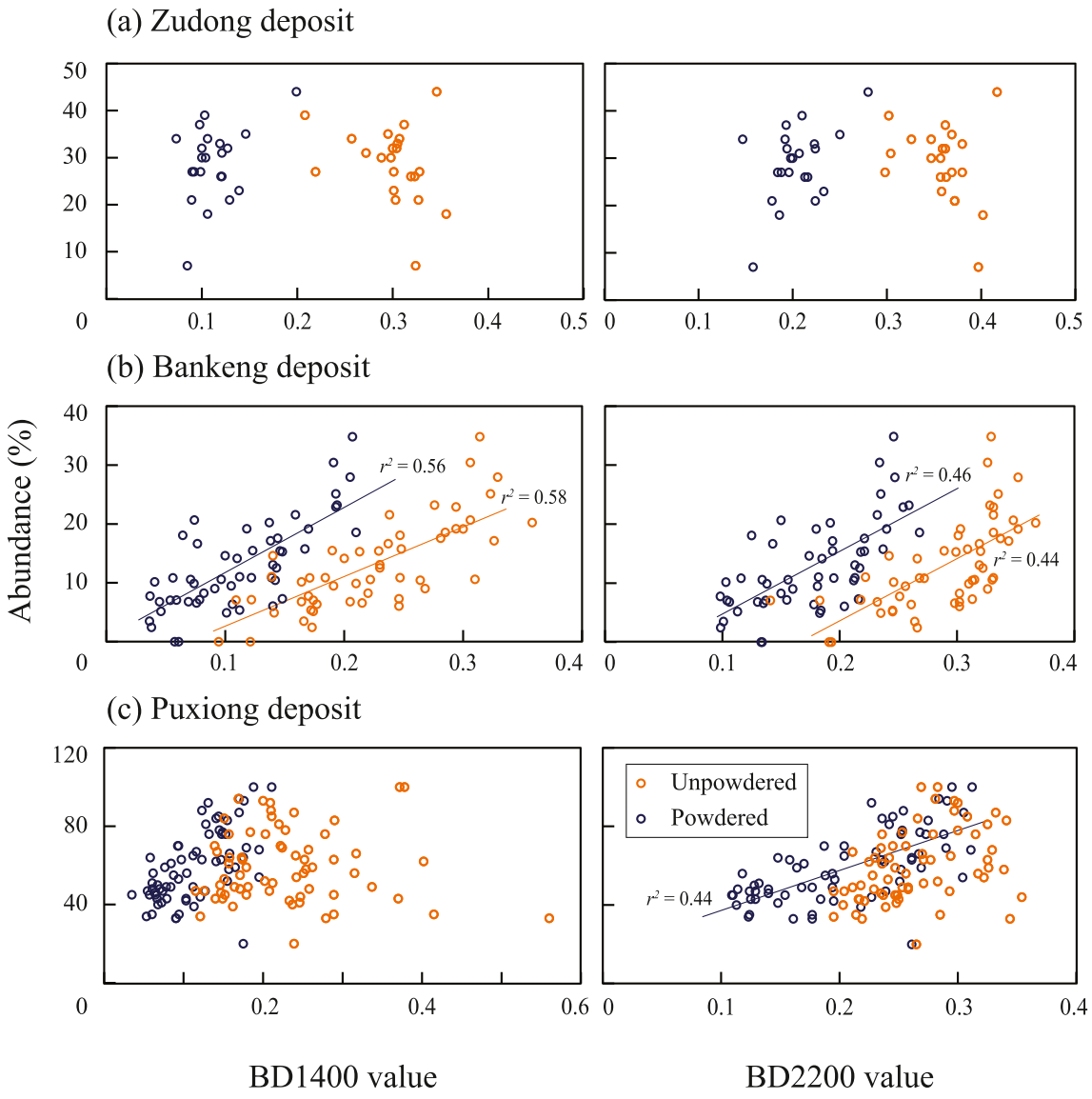

Fig. 8. Correlation between abundance of clay minerals and BD1400 and BD1900 values, respectively, of both unpowdered and powdered samples from the Zudong, Bankeng and Puxiong deposits.

Puxiong deposit, but only for the powdered samples (r^2 = ~0.4) (Figs. 8c). Likewise, results significantly vary when applying index M1390 to represent the abundance of kaolinite-group minerals. Powdered samples from Zudong give a poor correlation (r^2 = 0.34) but no correlation is shown for the unpowdered samples (Fig. 9a); both unpowdered and powdered samples from Bankeng exhibit moderate correlation (r^2 = ~0.5) (Fig. 9b); whereas only the powdered samples from Puxiong show a moderate correlation (r^2 = 0.62) but not the unpowdered samples (Fig. 9c). Given the fine grain size of clay minerals (Meunier, 2006), the grain size heterogeneity is expected to affect the reflectance (Hauff, 2005). Moreover, the QXRD analysis was undertaken on the powdered sample and a better match in grain size may explain the better correlations between the spectral reflectance of clay minerals in powdered samples and the QXRD results. However, profile-wise, the BD2200 and BD1400 values from the unpowdered samples show more systematic variations, especially in the deep Bankeng footslope profile and Puxiong profile, though the general trends exhibited from the unpowdered and powdered samples are consistent with each other (Figs. S1 – S8). Moreover, both indices show abrupt decreases across the pedolith-saprolite interface in these profiles, which is consistent with the typical observation that the pedolith-saprolite interface is a weathering front and more clay minerals would form in more weathered pedolith (Righi and Meunier, 1995; Velde and Meunier, 2008). Further, from our data, BD2200 apparently shows a better match, and would be a better proxy to indicate the abundance of clay minerals in regolith.

For the identification of clay minerals, the spectral index 2160D2190 can successfully indicate the dominance of kaolinite-group minerals in the clay mineral assemblage, in accordance with the results from XRD analysis. Furthermore, based on the clay separates from Zudong, the 2140D2190 ratio also shows moderately good correlations with the crystallinity we have determined based on the Hinckley index (r^2 = 0.5 for <2 μm-sized clay minerals and 0.6 for 2–20 μm-sized clay minerals, excluding an outliner from the lower saprolite) (Fig. 10). This demonstrates the applicability of VNIR-SWIR to evaluate the crystallinity of kaolinite-group minerals (Haest et al., 2012). On the other hand, the identification of illite could be difficult as the characteristic absorption bands of kaolinite significantly overlap with those of illite (cf. Bishop et al., 2008), and the dominance of kaolinite in most samples may mask the spectral features of illite for identification. The BD2350 shows moderate correlation (r^2 = 0.33) against the illite abundance for the Puxiong deposit (Fig. 11a), suggesting that it could potentially identify illite when the content is high. However, the 2350De index suggests that

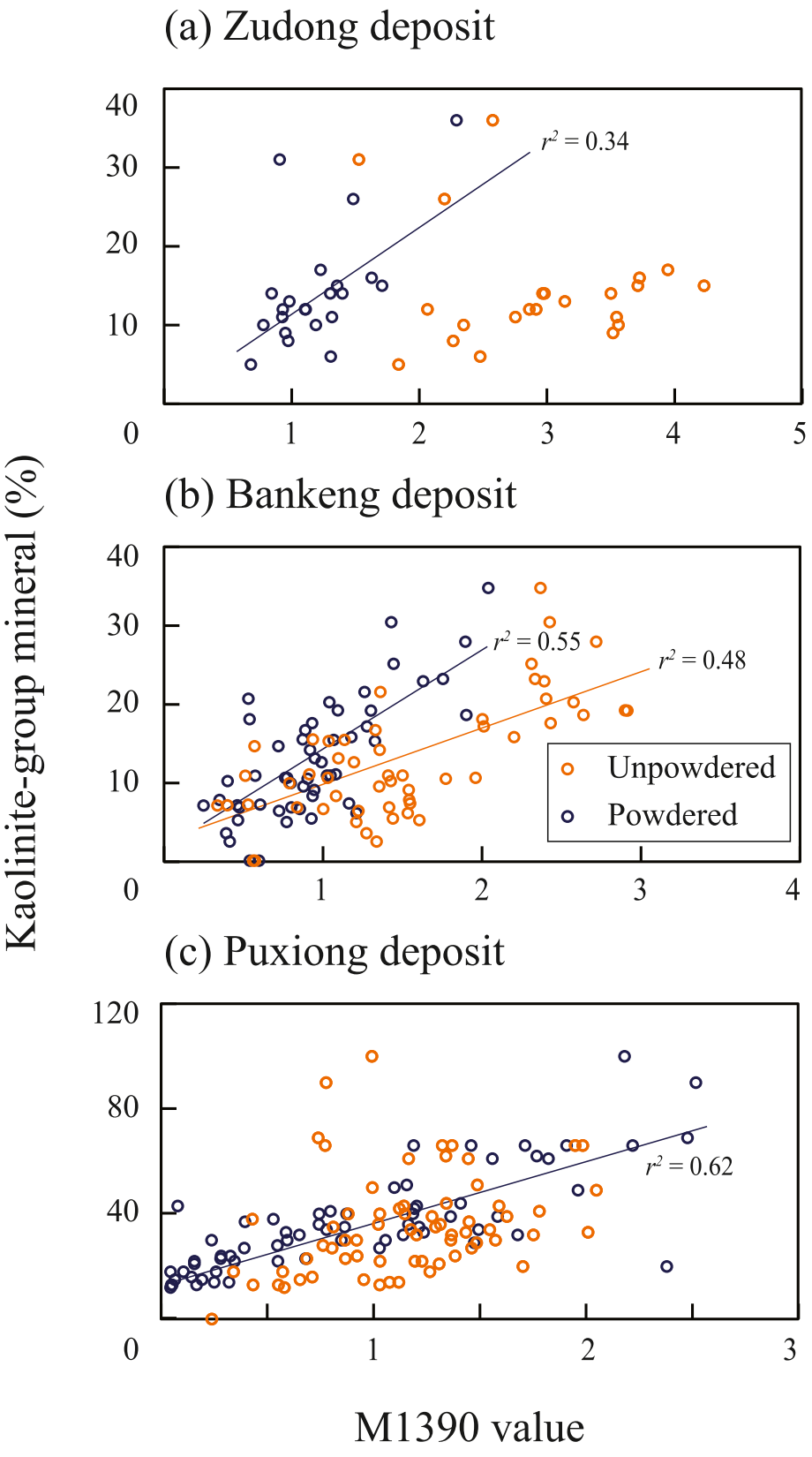

Fig. 9. Correlation between the abundance of kaolinite-group minerals and M1390 values of both unpowdered and powdered samples from the Zudong, Bankeng and Puxiong deposits.

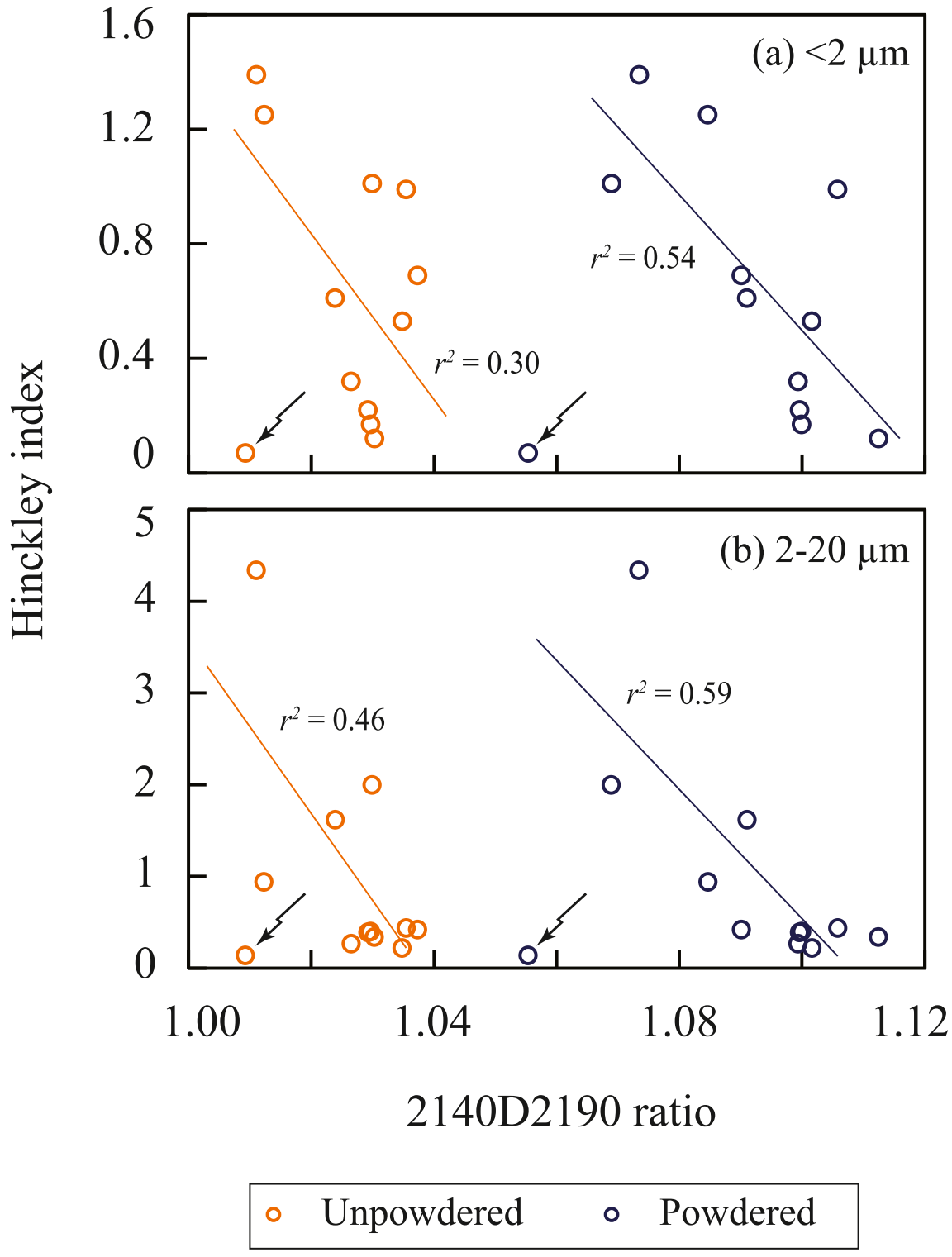

Fig. 10. Correlation between the Hinckley index of the kaolinite-group minerals (data from Li and Zhou, 2020) and the 2140D2190 ratios for particle size of (a) <2 μm and (b) 2–20 μm from the Zudong deposit.

Al-smectite is more abundant than illite in the non-kaolinite group minerals, in contrary to the QXRD results. As the ~2350 nm adsorption band is often weakly developed for most samples, the differences between the reflectance of the four bands used for the 2350De index may not be large enough to define the index for an accurate separation.

5.2.2. Fe (oxyhydr)oxides

Two spectral indices, BD500 and BD900, are applied in this study to evaluate their applicability as proxies for Fe (oxyhydr)oxides. However, only in the unpowdered samples from Bankeng, BD500 value shows a moderate correlation with the bulk Fe content (r^2 = 0.4) (Fig. S9). The poor correlations are likely due to the overall low Fe content and low abundance of Fe (oxyhydr)oxides in the regolith. Moreover, the potential overlapping of absorption bands from the clay minerals at around 960 nm would cause problem in determining the band depth and position center for BD900 (Hunt, 1977; Hunt and Ashley, 1979). Therefore,

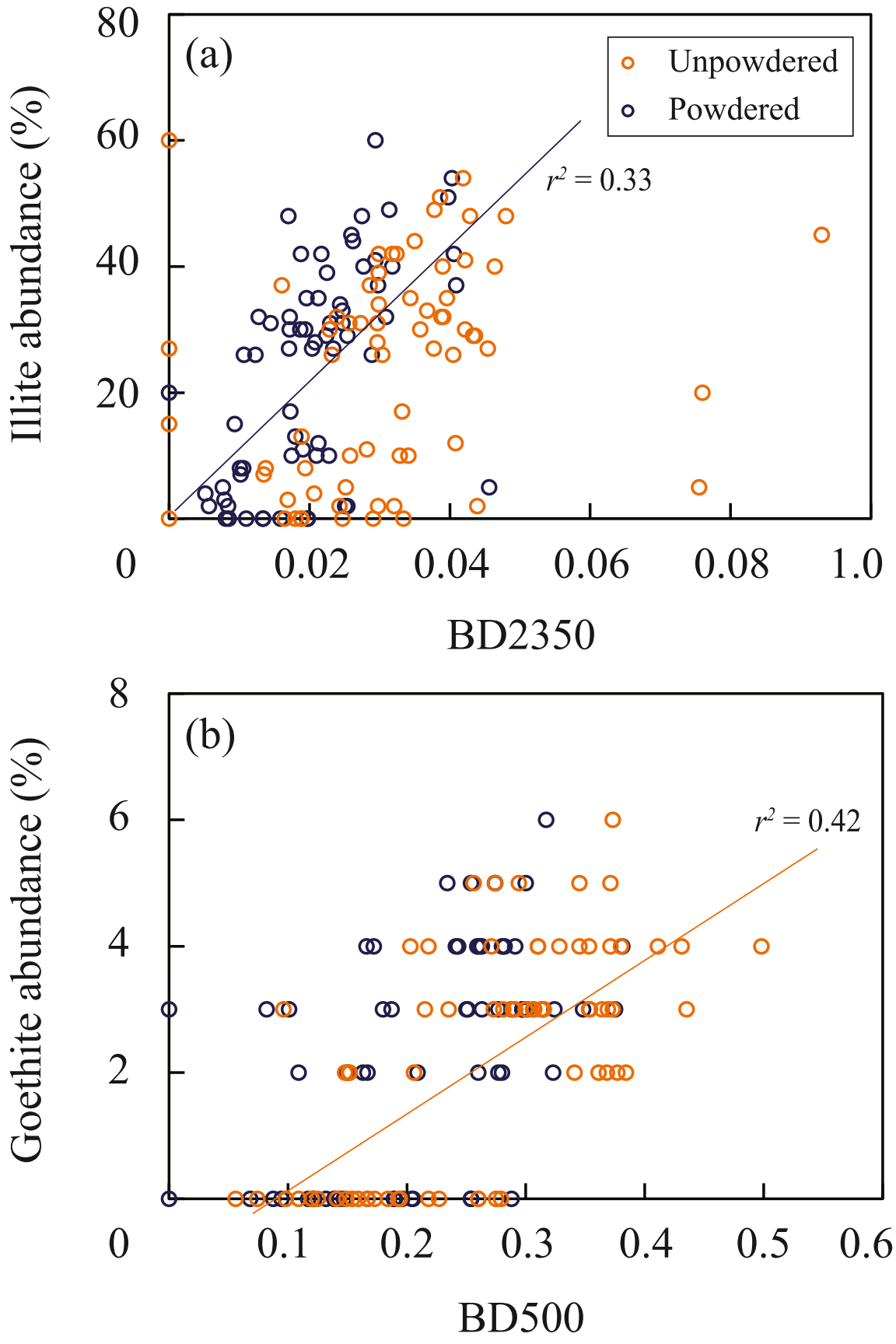

Fig. 11. Correlation between (a) the abundance of illite and BD2350 values and (b) the abundance of goethite and BD500 values of both unpowdered and powdered samples from the Puxiong deposit.

BD500 would be a more preferred index to estimate the abundance of Fe (oxyhydr)oxides and to determine the relative proportion of hematite and goethite. From the Puxiong profile, the BD500 value shows a moderate correlation with the abundance of goethite (r^2 = 0.4; Fig. 11b), and the position of the absorption band, 500 wvl, suggests that goethite is the major Fe (oxyhydr)oxide phase (Table S4 and S5), in agreement with the QXRD result. Although further studies on the Fe-poor regolith would be beneficial to evaluate the applicability of VNIR-SWIR to characterize Fe (oxyhydr)oxides in regolith, this study also agrees with previous studies (e.g., Liu et al., 2021; Tan et al., 2022) that BD500 could be a useful proxy to indicate the abundance and composition of Fe (oxyhydr)oxides in regolith.

5.3. Spectral proxies for REE concentration and occurrence

By comparing against the Nd concentrations measured by ICP-MS on acid-digested bulk regolith samples, we discovered that the Nd spectral features could show good correlations with the bulk Nd concentrations of samples from the Zudong and Bankeng deposits, but not for the Puxiong deposit. In this study, the difference between the maxima and associated minima in the second derivative curves (M797-M785 and M742-M730) are alternatively used to normalize all the data from different deposits, instead of the maxima alone. A correlation analysis shows that the numerical difference applied here would generally have a better correlation with the bulk Nd concentration compared to the maxima at the corresponding wavelength (Figs. 12, S10 and S11).

In both, the Zudong and Bankeng deposits, M797-M785 values have good correlations with bulk Nd (Zudong: r^2 = 0.71; Bankeng: r^2 = ~0.75 for both unpowdered and powdered samples) and REE (Zudong: r^2 = 0.68 for unpowdered samples; 0.61 for powdered samples; Bankeng: r^2 = 0.64) concentrations (Figs. 12a and b). For the Zudong deposit, M742-M730 values only show moderately good correlations for the unpowdered samples with the bulk Nd (r^2 = 0.58) and REE (r^2 = 0.49), if excluding an outliner (Sample LN-1-12) though the reason for outlining is unknown, however, M742-M730 values from the powdered samples could not be correlated with the bulk Nd and REE concentrations (Fig. S10). At Bankeng, the M742-M730 values show moderately good correlations with the bulk Nd (r^2 = ~0.55) and REE (r^2 = 0.46) concentrations for both unpowdered and powdered samples (Fig. S10). Profile-wise, variation of the M797-M785 values, from both unpowdered and powdered samples, mimic that of the Nd concentration in Zudong Profile LN-2 but deviated much in upper part (at depth shallower than 3.5 m) of the Zudong Profile LN-1 (Figs. S1 and S2). For the Bankeng profiles, variation of the M797-M785 values from the unpowdered samples demonstrate better matches with that of the bulk Nd concentration in the footslope and ridgetop profiles (Figs. S3 and S5),

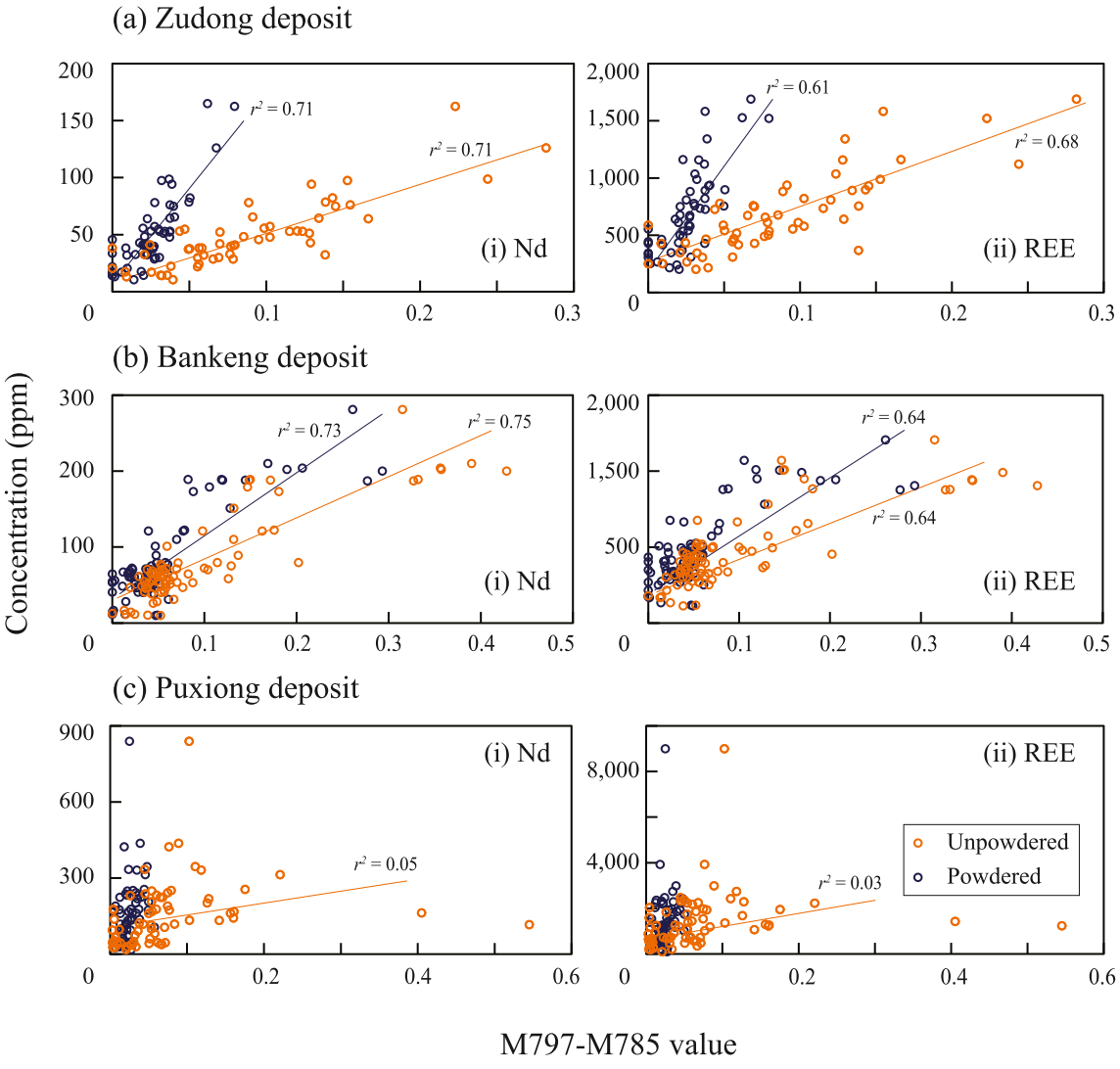

Fig. 12. Correlation between Nd and REE concentrations and M797-M785 values of both unpowdered and powdered samples from the Zudong, Bankeng and Puxiong deposits.

however interestingly, for the upslope profile, the vertical trend revealed from the powdered samples match better with that of the bulk Nd concentration (Fig. S4). In the Puxiong deposit, neither M797-M785 nor M742-M730 values show correlation with the bulk Nd or REE concentrations ($r^2 < 0.1$) (Figs. 12c and S5c). Likewise, the Nd concentration peak at the depth of 19 m is not picked up by the M797-M785 profiles though the unpowdered samples apparently recorded the other sub-ordinate concentration peaks of Nd at the depth of 26 and 41 m, respectively, in the saprolite (Fig. S7).

A couple of reasons could affect VNIR-SWIR spectral reflectance, including grain size heterogeneity, abundance of transparent and translucent phases, Fe content, and organic content (Hauff, 2005). In the Puxiong deposit, the spectral reflectance of Nd is generally weaker although the regolith derived from syenite is generally more homogeneous in grain size due to absence of quartz (Estrade et al., 2019; Wang et al., 2024). The low reflectance is likely due to broad spectral overlapping by Fe (oxyhydr)oxides over the range from 500 to 900 (Cudahy and Ramanaidou, 1997; Morris et al., 1985). The Fe content of the Puxiong deposit (4.5 wt% Fe_2O_3 on average; Table S3) is much higher than the other two deposits and goethite is consistently detected by XRD in the profile. Notably for the samples with Fe_2O_3 content below 3 wt%, they show moderate correlation between the M797-M785 value and Nd concentration ($r^2 = \sim 0.5$, based on 8 samples), and a better correlation may be constructed if the database is to be enlarged. This illustrates that the application of M797-M785 as proxy for Nd and REE concentrations in low-grade regolith-hosted REE deposits is only effective in low Fe regolith. The occurrence of Fe (oxyhydr)oxides could also explain why the M797-M785 and M742-M730 values obtained from the powdered samples often fail to indicate the bulk Nd and REE concentration. As the total amount of Fe (oxyhydr)oxides is generally low in the studied deposits, powdering would homogenize the distribution of Fe (oxyhydr) oxides and make the effect of Fe (oxyhydr)oxides on spectral reflectance of Nd more extensive throughout the whole sample, particularly considering that reflectance spectroscopy is a surface analysis technique with a vertical profiling of only a few ten micrometers.

For the Bankeng upslope profile, we postulate the relatively high abundance of translucent coarse quartz grains may degrade the spectral reflectance thus the M797-M785 values obtained from the unpowdered samples are less indicative to the bulk Nd concentration than those from the powdered samples. It is shown that coarse quartz grain sizes could dampen the relationship between the absorption features of kaolinite and its abundance (Laukamp et al., 2021). Also, the sensitivity of phyllosilicates would be greatly enhanced when coarse grains of quartz are present to increase the 'optical depth' of the samples, causing an overestimation of these phyllosilicate phases (Uren et al., 2021). Although the influence on REE spectral features is not yet understood, we assume grain size of quartz would cause certain effect in a similar fashion. Moreover, the generally low Nd concentrations in the regolith-hosted REE deposits, especially for the HREE-enriched ones like the Zudong deposit, would also affect the reliability of the obtained M797-M785 and M742-M730 values.

To further evaluate the reliability of the use of Nd spectral intensity to estimate the Nd concentration in low-Fe regolith, we calculated the correlation coefficient (r^2) between the M797-M785 value and Nd concentration adopting the Zudong and Bankeng samples, which show less influence by the existence of Fe (oxyhydr)oxides. Starting from the detection limit of 50 ppm as suggested by Tan et al. (2022), we eliminate the samples containing <50 ppm Nd stepwise in interval of 10 ppm from the calculation to trace the changes in correlation. The result shows that only the removal of samples with Nd concentration < 10 ppm would enhance the correlation (Table S6). Further to test whether the Nd spectral feature could be applied as a semi-quantitative indicator, linear regression is performed on the M797-M785 values to predict the Nd concentrations in the samples from the Zudong and Bankeng deposits as these samples are largely free of the effect of Fe^{3+}. We applied the unpowdered samples from these two deposits for the regression and a moderately good correlation is shown between the predicted and the ICPMS-measured Nd concentration ICPMS ($r^2 = 0.69$), with a root mean square error (RMSE) of 28 ppm (Fig. 13). This further proves the applicability of VNIR-SWIR in estimating the regolith-hosted REE concentrations.

The adsorption band position of REE could shift (for <20 nm) in accordance to the bonding ligand and coordination symmetry (Dijkstra et al., 2024). In this study, the Nd^{3+} absorption bands positioned at 742 and 797 nm (Figs. 5–7) are more close to those of bastnäsite (Turner et al., 2016) than the other REE phases previously determined in the literature. This implies that REE may occur as carbonate phases in the regolith, however, that is not supported by our previous mineralogical studies on these deposits (Li et al., 2019, 2020; Wang et al., 2024). Alternatively, part of adsorbed REE could occur as carbonate complex, as suggested by Li et al. (2022), for the REE carbonate-like band position. Nonetheless, it should also be noted that a 1- to 3-nm differences in the values of VNIR-SWIR absorption bands happen among instruments, even when analyzing the same mineral grains, and that would be large enough to cover various bonding environment of the REE (cf. Dijkstra et al., 2024; Turner et al., 2014, 2016, 2018).

5.4. Limitation

Even though VNIR-SWIR spectroscopy has been demonstrated to be applicable for semi-quantitative estimation of Nd concentration and abundance of kaolinite-group minerals, and evaluation of other mineralogical properties and weathering intensity of regolith, there are some key constraints on the application of VNIR-SWIR spectroscopy to the exploration of regolith-hosted REE resources. One key constraint is the Fe content of the regolith. From the Puxiong samples, it is notable that Fe^{3+} can impose a significant spectral overlapping and mask the spectral features of Nd^{3+}, even when the bulk Nd concentration of the Puxiong samples is the highest among the three studied deposits. VNIR-SWIR spectroscopy would be more efficient on exploring Fe-poor regolith-hosted REE resources. Also, it is likely that VNIR-SWIR spectroscopy is more applicable to granite-derived regolith compared to syenite-derived, and probably volcanic rock-derived regolith, as the fine-grained nature of the later would intensify the effect of Fe^{3+} on the resolution of Nd^{3+} spectral features. Moreover, as only Nd could generally give reliable spectral features in regolith-hosted REE deposits, of which the REE grade is comparatively low, the determination of the REE pattern would deem to be impossible, limiting the technique in targeting HREE-rich resources. Nonetheless, as a potential field-based technique to be capable of rapid semi-quantification of REE concentrations in regolith, VNIR-SWIR spectroscopy will still be very beneficial to future exploration of regolith-hosted REE resources.

6. Conclusion

The applicability of VNIR-SWIR spectroscopy as a potential rapid and semi-quantitative field-based technique for reconnaissance of regolith-hosted REE resources is evaluated with three world-class regolith-hosted REE deposits, of different REE composition, protolith, and clay mineralogy, in South China. The intensity of ~800 nm absorption band from Nd^{3+} is able to semi-quantitatively indicate the Nd concentration, that in turn represents the total REE, in regolith, despite constraint by the Fe content. It is noted that Fe_2O_3 content higher than 3 wt% in the regolith would significantly mask the spectral features of Nd^{3+}, disabling the usage of these spectral features to indicate the Nd concentration. On the other hand, VNIR-SWIR spectroscopy also shows its ability to identify kaolinite-group mineral-rich regolith and further to indicate the crystallinity of these major REE sorbents in regolith-hosted REE resources. Information beneficial to resources exploration, such as the weathering intensity and abundance of Fe (oxyhydr)oxide phases of regolith, can also be obtained from the VNIR-SWIR spectra. Furthermore, we demonstrate the applicability of VNIR-SWIR spectroscopy to

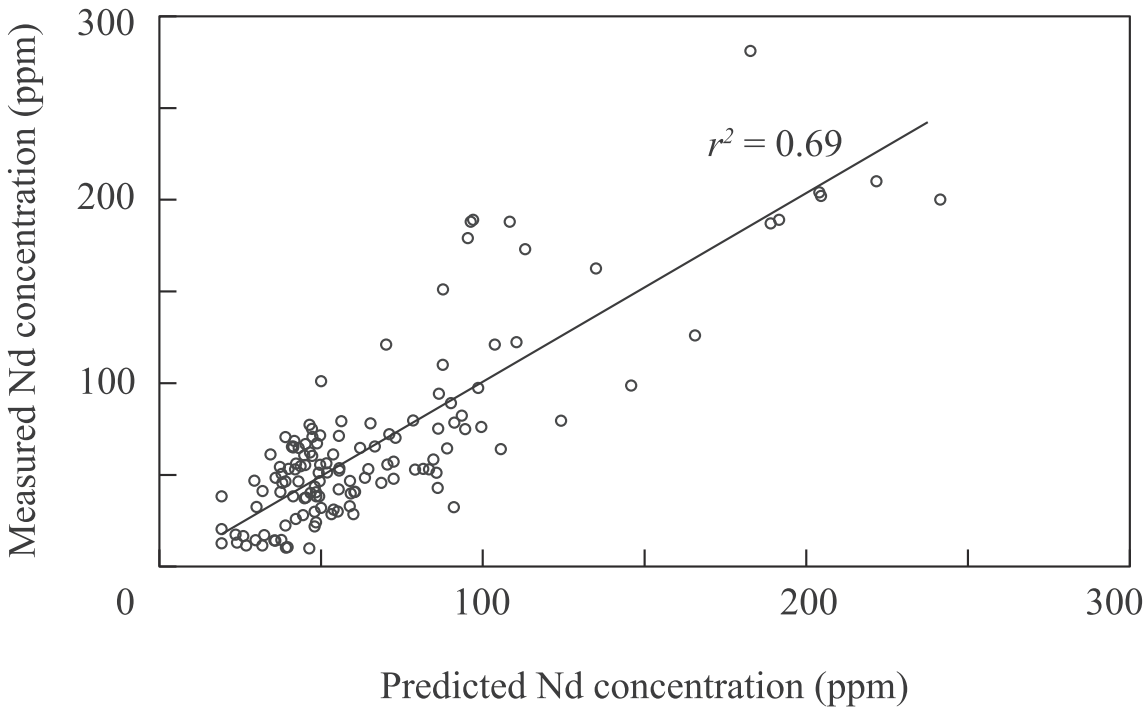

Fig. 13. Correlation between the measured Nd concentration from ICPMS and predicted Nd concentration from the M797-M785 value of samples from the Zudong and Bankeng deposits.

heterogeneous field samples. The application of VNIR-SWIR spectroscopy as a rapid and reliable field-based tool for preliminary regolith surveying for REE resources is feasible and would greatly assist the planning of subsequent exploration works, such as drilling, sampling, and resources evaluation.

CRediT authorship contribution statement

Martin Yan Hei Li: Writing – review & editing, Writing – original draft, Visualization, Methodology, Investigation, Formal analysis, Conceptualization. **Jiacheng Liu:** Writing – review & editing, Methodology, Investigation, Formal analysis, Conceptualization. **Wei Tan:** Writing – review & editing, Formal analysis. **Jia-Xi Zhou:** Writing – review & editing, Funding acquisition. **Mei-Fu Zhou:** Writing – review & editing, Supervision, Funding acquisition.

Declaration of competing interest

All authors declare that they have no known conflict of interest or personal relationships that could have appeared to influence the work reported in this paper.

Data availability

Data will be made available on request.

Acknowledgements

We thank Mr. Rhys Ngan and Mr. Ken Lo for assistance in sample preparation, and Mr. Xiaorong Qin and Mr. Mengqi Han for assistance in spectral measurement. The weather of the days when the first author, Martin Li, sampled the Bankeng profiles was disastrous, and he is indebted to Dr. Winston Zhao for having him throughout the field work. We also thank the editorial handling by Profs. Stefano Albanese and David Cohen and the constructive comments by the two anonymous reviewers. This study was supported financially by the Natural Science Foundation of China (Grant No. 92162323 and 42302264) and a Key Basic Research Project of Yunnan Province (Grant No. 202401AS070127).

Appendix A. Supplementary data

Supplementary data to this article can be found online at https://doi.org/10.1016/j.gexplo.2024.107578.

References

Adams, J.W., 1965. The visible region absorption spectra of rare-earth minerals. Am. Mineral. 50, 356–366.
Bishop, J., Lane, M., Dyar, M., Brown, A., 2008. Reflectance and emission spectroscopy study of four groups of phyllosilicates: smectites, kaolinite-serpentines, chlorites and micas. Clay Miner. 43, 35–54.
Boesche, N.K., Rogass, C., Lubitz, C., Brell, M., Herrmann, S., Mielke, C., Tonn, S., Appelt, O., Altenberger, U., Kaufmann, H., 2015. Hyperspectral REE (rare earth element) mapping of outcrops—applications for neodymium detection. Remote Sens. 7, 5160–5186.
Booysen, R., Jackisch, R., Lorenz, S., Zimmermann, R., Kirsch, M., Nex, P.A., Gloaguen, R., 2020. Detection of REEs with lightweight UAV-based hyperspectral imaging. Sci. Rep. 10, 17450.
Borst, A.M., Smith, M.P., Finch, A.A., Estrade, G., Villanova-de-Benavent, C., Nason, P., Marquis, E., Horsburgh, N.J., Goodenough, K.M., Xu, C., 2020. Adsorption of rare earth elements in regolith-hosted clay deposits. Nat. Commun. 11, 1–15.
Chang, Z., Yang, Z., 2012. Evaluation of inter-instrument variations among short wavelength infrared (SWIR) devices. Econ. Geol. 107, 1479–1488.
Clark, R., 1995. Reflectance spectra, rock physics and phase relations. In: Handbook of Physical Constants. American Geophysical Union.
Clark, R.N., King, T.V., Klejwa, M., Swayze, G.A., Vergo, N., 1990. High spectral resolution reflectance spectroscopy of minerals. J. Geophys. Res. Solid Earth 95, 12653–12680.
Coppin, F., Berger, G., Bauer, A., Castet, S., Loubet, M., 2002. Sorption of lanthanides on smectite and kaolinite. Chem. Geol. 182, 57–68.
Cuadros, J., Sánchez-Marañón, M., Mavris, C., Fiore, S., Bishop, J.L., Melgosa, M., 2020. Color analysis and detection of Fe minerals in multi-mineral mixtures from acid-alteration environments. Appl. Clay Sci. 193, 105677.
Cudahy, T., Ramanaidou, E., 1997. Measurement of the hematite: goethite ratio using field visible and near-infrared reflectance spectrometry in channel iron deposits, Western Australia. Aust. J. Earth Sci. 44, 411–420.
Dijkstra, A., Bakker, W., Deon, F., Marcatelli, C., Plokker, M., Hintzen, H., 2024. Identification of rare earth elements in synthetic and natural monazite and xenotime by visible-to-shortwave infrared reflectance spectroscopy. Phys. Chem. Miner. 51, 1–19.

Estrade, G., Marquis, E., Smith, M., Goodenough, K., Nason, P., 2019. REE concentration processes in ion adsorption deposits: evidence from the Ambohimirahavavy alkaline complex in Madagascar. Ore Geol. Rev. 103027.
Fu, W., Luo, P., Hu, Z., Feng, Y., Liu, L., Yang, J., Feng, M., Yu, H., Zhou, Y., 2019. Enrichment of ion-exchangeable rare earth elements by felsic volcanic rock weathering in South China: genetic mechanism and formation preference. Ore Geol. Rev. 114, 103120.
Haest, M., Cudahy, T., Laukamp, C., Gregory, S., 2012. Quantitative mineralogy from infrared spectroscopic data. I. Validation of mineral abundance and composition scripts at the rocklea channel iron deposit in Western Australia. Econ. Geol. 107, 209–228.
Hauff, P.L., 2005. Applied reflectance spectroscopy; with emphasis on data collection and data interpretation using field spectrometers. In: Spectral International Incorporated Version 4.
Huang, J., He, H., Tan, W., Liang, X., Ma, L., Wang, Y., Qin, X., Zhu, J., 2021. Groundwater controls REE mineralisation in the regolith of South China. Chem. Geol. 577, 120295.
Hunt, G.R., 1970. Visible and near-infrared spectra of minerals and rocks: I silicate minerals. Mod. Geol. 1, 283–300.
Hunt, G.R., 1977. Spectral signatures of particulate minerals in the visible and near infrared. Geophysics 42, 501–513.
Hunt, G.R., Ashley, R.P., 1979. Spectra of altered rocks in the visible and near infrared. Econ. Geol. 74, 1613–1629.
IEA, 2021. Global Energy Review 2021, Paris.
Laukamp, C., Rodger, A., LeGras, M., Lampinen, H., Lau, I.C., Pejcic, B., Stromberg, J., Francis, N., Ramanaidou, E., 2021. Mineral physicochemistry underlying feature-based extraction of mineral abundance and composition from shortwave, mid and thermal infrared reflectance spectra. Minerals 11, 347.
Li, M.Y.H., Zhou, M.-F., 2020. The role of clay minerals in formation of the regolith-hosted heavy rare earth element deposits. Am. Mineral. 105, 92–108.
Li, M.Y.H., Zhou, M.-F., 2023. Physicochemical variation of clay minerals and enrichment of rare earth elements in regolith-hosted deposits: exemplification from the Bankeng deposit in South China. Clay Clay Miner. 71, 362–376.
Li, M.Y.H., Zhou, M.-F., 2024. Hyper-enrichment of heavy rare earth element in highly evolved granites through multiple hydrothermal mobilization. Am. Mineral. 109 https://doi.org/10.2138/am-2023-9117.
Li, Y.H.M., Zhao, W.W., Zhou, M.-F., 2017. Nature of parent rocks, mineralization styles and ore genesis of regolith-hosted REE deposits in South China: an integrated genetic model. J. Asian Earth Sci. 148, 65–95.
Li, M.Y.H., Zhou, M.-F., Williams-Jones, A.E., 2019. The genesis of regolith-hosted heavy rare earth element deposits: insights from the world-class Zudong deposit in Jiangxi Province, South China. Econ. Geol. 114, 541–568.
Li, M.Y.H., Zhou, M.-F., Williams-Jones, A.E., 2020. Controls on the dynamics of rare earth elements during sub-tropical hillslope processes and formation of regolith-hosted deposits. Econ. Geol. 115, 1097–1118.
Li, M.Y.H., Teng, F.-Z., Zhou, M.-F., 2021. Phyllosilicate controls on magnesium isotopic fractionation during weathering of granites: implications for continental weathering and riverine system. Earth Planet. Sci. Lett. 553, 116613.
Li, M.Y.H., Kwong, H.T., Williams-Jones, A.E., Zhou, M.-F., 2022. The thermodynamics of rare earth element liberation, mobilization and supergene enrichment during groundwater-regolith interaction. Geochim. Cosmochim. Acta 330, 258–277.
Liu, G., 2005. Electronic Energy Level Structure, Spectroscopic Properties of Rare Earths in Optical Materials. Springer, pp. 1–94.
Liu, J., He, H., Michalski, J., Cuadros, J., Yao, Y., Tan, W., Qin, X., Li, S., Wei, G., 2021. Reflectance spectroscopy applied to clay mineralogy and alteration intensity of a thick basaltic weathering sequence in Hainan Island, South China. Appl. Clay Sci. 201, 105923.
Luo, L., Tan, W., Qin, X., Ji, S., Liang, X., He, H., 2024. Variation in the structural order of kaolinite in regolith as an effective indicator of REE mineralization. Clay Clay Miner. 72, e1.
Mathian, M., Hebert, B., Baron, F., Petit, S., Lescuyer, J.-L., Furic, R., Beaufort, D., 2018. Identifying the phyllosilicate minerals of hypogene ore deposits in lateritic saprolites using the near-IR spectroscopy second derivative methodology. J. Geochem. Explor. 186, 298–314.
Meunier, A., 2005. Clays. Springer Science & Business Media.
Meunier, A., 2006. Why are clay minerals small? Clay Miner. 41, 551–566.
Möller, V., Williams-Jones, A.E., 2018. A hyperspectral study (V-NIR-SWIR) of the Nechalacho REE-Nb-Zr deposit, Canada. J. Geochem. Explor. 188, 194–215.
Morris, R.V., Lauer Jr., H.V., Lawson, C.A., Gibson Jr., E.K., Nace, G.A., Stewart, C., 1985. Spectral and other physicochemical properties of submicron powders of hematite (α-Fe_2O_3), maghemite (γ-Fe_2O_3), magnetite (Fe_3O_4), goethite (α-FeOOH), and lepidocrocite (γ-FeOOH). J. Geophys. Res. Solid Earth 90, 3126–3144.
Neave, D.A., Black, M., Riley, T.R., Gibson, S.A., Ferrier, G., Wall, F., Broom-Fendley, S., 2016. On the feasibility of imaging carbonatite-hosted rare earth element deposits using remote sensing. Econ. Geol. 111, 641–665.
Nesbitt, H., Young, G.M., 1989. Formation and diagenesis of weathering profiles. J. Geol. 97, 129–147.
Riesgo García, M.V., Krzemień, A., del Campo, M.Á.M., Álvarez, M.M., Gent, M.R., 2017. Rare earth elements mining investment: it is not all about China. Res. Policy 53, 66–76.
Righi, D., Meunier, A., 1995. Origin of Clays by Rock Weathering and Soil Formation, Origin and Mineralogy of Clays: Clays and the Environment. Springer, pp. 43–161.
Rowan, L.C., Kingston, M.J., Crowley, J.K., 1986. Spectral reflectance of carbonatites and related alkalic igneous rocks; selected samples from four North American localities. Econ. Geol. 81, 857–871.
Sherman, D.M., Waite, T.D., 1985. Electronic spectra of Fe3+ oxides and oxide hydroxides in the near IR to near UV. Am. Mineral. 70, 1262–1269.
Tamer, M., 2013. Quantitative Phase Analysis Based on Rietveld Structure Refinement for Carbonate Rocks.
Tan, W., Qin, X., Liu, J., Michalski, J., He, H., Yao, Y., Yang, M., Huang, J., Lin, X., Zhang, C., 2021. Visible/near infrared reflectance (VNIR) spectral features of ion-exchangeable rare earth elements hosted by clay minerals: potential use for exploration of regolith-hosted REE deposits. Appl. Clay Sci. 215, 106320.
Tan, W., Qin, X., Liu, J., Zhou, M.-F., He, H., Wang, C.Y., Huang, J., Zhu, J., Yao, Y., Cudahy, T., 2022. Feasibility of visible short-wave infrared reflectance spectroscopy to characterize regolith-hosted rare earth element mineralization. Econ. Geol. 117, 495–508.
Turner, D.J., Rivard, B., Groat, L.A., 2014. Visible and short-wave infrared reflectance spectroscopy of REE fluorocarbonates. Am. Mineral. 99, 1335–1346.
Turner, D.J., Rivard, B., Groat, L.A., 2016. Visible and short-wave infrared reflectance spectroscopy of REE phosphate minerals. Am. Mineral. 101, 2264–2278.
Turner, D.J., Rivard, B., Groat, L.A., 2018. Visible and short-wave infrared reflectance spectroscopy of selected REE-bearing silicate minerals. Am. Mineral. 103, 927–943.
Uren, A.L., Laukamp, C., George, A.D., Occhipinti, S.A., Aitken, A.R., 2021. Inferring sandstone grain size using spectral datasets: an example from the Bresnahan Group, Western Australia. Remote Sens. Environ. 252, 112109.
Velde, B.B., Meunier, A., 2008. The Origin of Clay Minerals in Soils and Weathered Rocks. Springer Science & Business Media.
Viviano, C.E., Seelos, F.P., Murchie, S.L., Kahn, E.G., Seelos, K.D., Taylor, H.W., Taylor, K., Ehlmann, B.L., Wiseman, S.M., Mustard, J.F., 2014. Revised CRISM spectral parameters and summary products based on the currently detected mineral diversity on Mars. Journal of Geophysical Research: Planets 119, 1403–1431.
Wang, C., Zhang, T., Pan, X., 2017. Potential of visible and near-infrared reflectance spectroscopy for the determination of rare earth elements in soil. Geoderma 306, 120–126.
Wang, M., Li, M.Y.H., Zhou, M.-F., Zhou, J.-X., Sun, G., Zhou, Y., Li, Y., 2024. Enrichment of rare earth elements during the weathering of alkaline igneous systems: Insights from the Puxiong regolith-hosted REE deposit, SW China. Econ. Geol. 119, 161–187.
Xie, Y., Hou, Z., Goldfarb, R.J., Guo, X., Wang, L., 2016. Rare earth element deposits in China. Rev. Econ. Geol. 18, 115–136.
Yang, M., Liang, X., Ma, L., Huang, J., He, H., Zhu, J., 2019. Adsorption of REEs on kaolinite and halloysite: a link to the REE distribution on clays in the weathering crust of granite. Chem. Geol. 525, 210–217.
Zhou, M.F., Li, M.Y.H., Wang, Z., Li, X.C., Liu, J., 2020. The genesis of regolith-hosted rare earth element and scandium deposits: current understanding and outlook to future prospecting. Chin. Sci. Bull. 65, 3809–3824.